Training-Free Label Space Alignment for Universal Domain Adaptation

Dujin Lee[a], Sojung An[a], Jungmyung Wi[a], Kuniaki Saito[b], Donghyun Kim[a,*]

[a]*Department of Artificial Intelligence, Korea University, Republic of Korea*
[b]*OMRON SINIC X, Japan*

Abstract

Universal domain adaptation (UniDA) transfers knowledge from a labeled source domain to an unlabeled target domain, where label spaces may differ and the target domain may contain private classes. Previous UniDA methods primarily focused on visual space alignment but often struggled with visual ambiguities due to content differences, which limited their robustness and generalizability. To overcome this, we introduce a novel approach that leverages the strong *zero-shot capabilities* of recent vision-language foundation models (VLMs) like CLIP, concentrating solely on label space alignment to enhance adaptation stability. CLIP can generate task-specific classifiers based only on label names. However, adapting CLIP to UniDA is challenging because the label space is not fully known in advance. In this study, we first utilize generative vision-language models to identify unknown categories in the target domain. Noise and semantic ambiguities in the discovered labels—such as those similar to source labels (e.g., synonyms, hypernyms, hyponyms)—complicate label alignment. To address this, we propose a training-free label-space alignment method for UniDA (TLSA). Our method aligns label spaces instead of visual spaces by filtering and refining noisy labels between the domains. We then construct a *universal classifier* that integrates both shared knowledge and target-private class information, thereby improving generalizability under domain shifts. The results reveal that the proposed method considerably outperforms existing UniDA techniques across key DomainBed benchmarks, delivering an average improvement of +7.9%in H-score and +6.1% in H^3-score. Furthermore, incorporating self-training further enhances performance and achieves an additional (+1.6%) increment in both H- and H^3-scores.

Keywords:
Universal Domain Adaptation, Vision-Language Models, Foundation Models, Robustness, Self-training

1. Introduction

Domain shift remains a pivotal challenge, addressing the discrepancies between data distributions in real-world applications and training environments. Unsupervised domain adaptation (UDA) (Long et al., 2015; Ganin et al., 2016; Saito et al., 2018) aims to transfer knowledge from a labeled source domain to an unlabeled target domain, based on the stringent assumption that the label space remains unchanged across domains. However, in practical settings, the target label space may comprise only a subset of source classes that overlap with both domains or include target-exclusive classes unique to the target domain. Various studies have explored these complexities. Open-set domain adaptation (ODA) and partial-set domain adaptation (PDA) assume that the label space of each domain is a subset of another's (Panareda Busto and Gall, 2017; Cao et al., 2018). Nonetheless, these approaches depend on prior knowledge of label-space shifts, limiting their real-world applicability. To address this constraint, Universal Domain Adaptation (UniDA) was introduced (You et al., 2019a; Saito et al., 2020) for broader applicability.

In UniDA, a primary challenge is distinguishing target-private samples from source-private ones. Numerous studies have proposed innovative detection criteria utilizing entropy (Saito et al., 2020; Qu et al., 2023a), binary classifiers (Saito and Saenko, 2021; Lu et al., 2024), optimal transport (Chang et al., 2022), energy-based methods (Chen et al., 2022a), class prototypes (Li et al., 2021a; Lai et al., 2023), and calibration techniques (Deng and Jia, 2023).Despite their capabilities, these methods struggle to differentiate between known and unknown classes that exhibit visual ambiguity due to content discrepancies across domains. This challenge arises because they rely on the geometric structure of visual features under domain shifts.

This study addresses these limitations by focusing exclusively on label-space alignment. To achieve this, we leverage the robust zero-shot capabilities of Vision-Language Models (VLMs) such as CLIP (Radford et al., 2021) and ALIGN (Li et al., 2021b). For instance, CLIP effectively recognizes diverse classes across domains by prompting label names through its fixed text encoder. To evaluate this ability, we conducted a pilot study assessing the performance of a zero-shot classifier across various label spaces within the UniDA framework. As shown in Fig. 1, zero-shot classifiers using customized label spaces exhibit substantial improvements in UniDA performance. Notably, simply incorporating oracle target private class names into the zero-shot classifier significantly outperformed state-of-the-art UniDA methods without requiring additional fine-

*Corresponding author
Email address: d_kim@korea.ac.kr (Donghyun Kim)

tuning. These findings suggest that addressing the UniDA problem is more efficiently achieved by aligning label spaces rather than visual spaces across domains when utilizing VLMs. Moreover, the generated textual outputs are directly inspectable, enhancing the explainability and interpretability of the proposed pipeline.

Inspired by Fig. 1, we aim to identify target private classes and obtain an empirical version of these classes, termed *predicted target private labels*, by employing generative VLMs (Li et al., 2022, 2023). A similar approach is utilized in ODA (Zara et al., 2023), which discovers target private labels through text-to-text matching between the two domains at the cluster level. Nevertheless, this method is highly dependent on clustering quality. Moreover, texts identified from the source domain often lack informativeness due to domain shifts, particularly regarding abstract classes (Section 2.3). In contrast, we propose removing labels containing source-related information by conducting instance-level discovery exclusively on texts from the target domain.

However, determining whether discovered labels include source-related information remains challenging due to noise (Fig. 2a) and semantic ambiguities, such as hyponyms (Fig. 2b) and synonyms (Fig. 2c)). For example, in Fig. 2b, the generative VLM outputs "Panasonic," a hyponym of "Monitor" in the source labels. Without proper alignment, "Panasonic" is incorrectly predicted as a target private label, leading to degraded performance.

To address this, we introduce **T**raining-free **L**abel **S**pace **A**lignment for UniDA (**TLSA**). Specifically, we first identify the raw labels of the target samples using a generative VLM. Subsequently, we implement three steps to eliminate incorrect or semantically ambiguous discovered labels from the source labels and accurately predict the true target private labels: (i) Synonym label alignment (Section 3.3), which identifies synonyms in raw discovered labels using WordNet and aligns them with the source labels to remove synonyms; (ii) Semantic label alignment (Section 3.4). To resolve the ambiguous similarity between source and discovered labels, we identify a set of predictions that are considered correct for an image within the CLIP joint embedding space. When this set lacks source labels and contains only discovered labels, we select only the filtered discovered labels as candidate labels. (iii) Frequency-based noise-candidate filtering (Section 3.5). To eliminate residual noise, we monitor the frequency of target private candidate labels that pass previous filters across the entire target domain, removing noisy candidate labels based on their occurrence patterns. Ultimately, we obtain the predicted target private labels used to construct a universal classifier alongside the source labels. Our universal classifier more effectively differentiates between known and unknown labels than methods that depend on the geometric structure of visual representations (Chang et al., 2022; Lai et al., 2023; Wang et al., 2024a). Additionally, our model demonstrates further performance enhancements when integrated with self-training (Section 3.6).

To validate our approach, we conducted experiments on four standard UniDA benchmarks, each representing a unique visual recognition domain-adaptation task. In summary, our contributions are:

1. We introduce a novel UniDA method by utilizing generative vision-language models to discover candidate target private classes through our filtering techniques.
2. By applying the filtered target private classes, we improve the CLIP zero-shot classifier for UniDA, termed the universal classifier.
3. Even without additional training, our approach achieves exceptionally strong performance compared to baselines.
4. We enhance the universal classifier through self-training to achieve full adaptation to the target domain.
5. We perform comprehensive analyses to validate the effectiveness of our approach, attaining state-of-the-art performance on H-score and H^3-score metrics.

Furthermore, as demonstrated in prior studies, fine-tuning the backbone CLIP on source data diminishes its ability to detect target private classes (Deng and Jia, 2023). This issue, known as *feature distortion* (Kumar et al., 2022; Shu et al., 2022; Trivedi et al., 2023; Saito et al., 2023), arises when the source data is used for tuning. Our method circumvents tuning on the source data by leveraging the source label space to filter and identify target private labels from the generative VLM. Consequently, our approach prevents feature distortion, enabling faster experimentation and improved performance.

2. Related Work

2.1. Vision-Language Models

Vision-language models have recently demonstrated great potential in learning generic visual representations. (Radford et al., 2021; Li et al., 2021b; Zhou et al., 2022). Their transferability is attributed to the ability to inject rich information into the model by aligning image-text pairs, rather than just a single word label. For example, CLIP (Radford et al., 2021) and ALIGN (Jia et al., 2021) demonstrate strong zero-shot performance in visual recognition. Not surprisingly, many studies have achieved high performance within only zero-shot pipelines by using the Vision-Language Models (VLMs) (Adila et al., 2023; Ge et al., 2023; Qu et al., 2024a; Zhao et al., 2024; Zanella and Ben Ayed, 2024; Wang et al., 2024b). Generative VLMs, including BLIP (Li et al., 2022, 2023), GPT-4 (Achiam et al., 2023), and LLaVA (Liu et al., 2024), have demonstrated strong performance on a wide range of vision–language generation tasks. In light of the latest advancements, we utilize BLIP to discover a label agnostic to the source domain for unlabeled target domain samples.

2.2. Universal Domain Adaptation

Unlike UDA, UniDA assumes a distinct scenario where the label set of the target domain may partially intersect with that of the source domain. Determining whether a given data belongs to a known or unknown class is a highly challenging task because the model can only predict the classes it is trained on. Therefore, baseline methods for UDA, such as adversarial learning (Ganin et al., 2016; Tzeng et al., 2017; Long et al.,

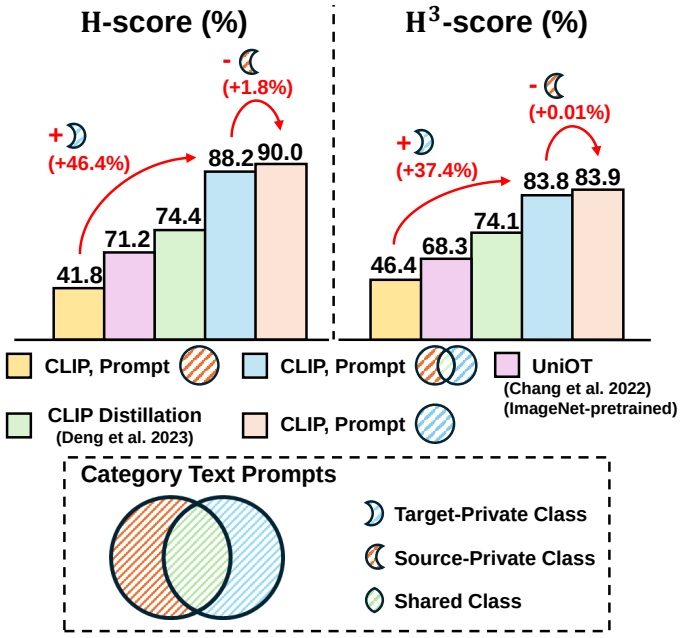

Figure 1: Comparison between CLIP Prompt and state-of-the-art methods on H-score and H^3-score. Our method achieves superior performance without additional training.

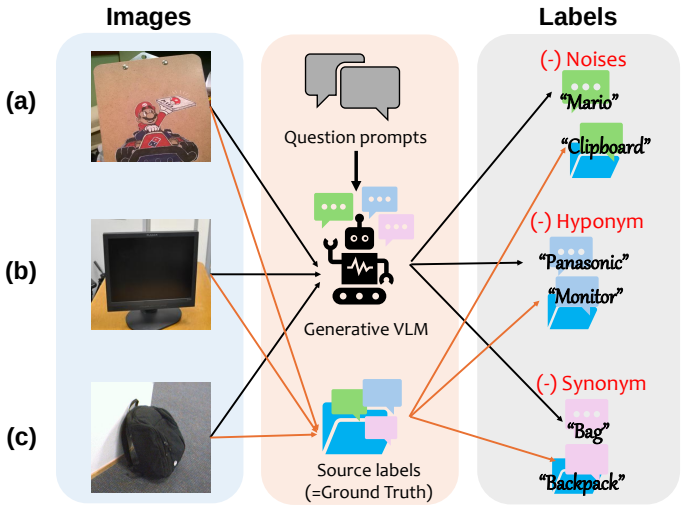

Figure 2: Examples of semantic ambiguity in generative VLM outputs: (a) noisy response, (b) hyponym prediction, and (c) synonym prediction.

2018) and metric learning (Long et al., 2015, 2017), lead to degradation in performance. The problem occurs because domain alignment is attempted without considering the possibility that the label space might differ, leading to negative transfer.

With the recent progress of VLMs, there has been growing recognition of the relatively limited exploration compared to pretrained backbones on ImageNet (Russakovsky et al., 2015) such as ResNet (He et al., 2016) and ViT (Dosovitskiy et al., 2020). In response, CLIP-Distillation (Deng and Jia, 2023) was proposed, utilizing foundation models (Radford et al., 2021; Oquab et al., 2023) trained on large datasets through self-supervised learning. This approach achieved state-of-the-art performance among CLIP-pretrained backbones by performing auto-calibration via learning the classifier temperature. Similarly, MemSPM (Lai et al., 2023) adopts a memory-based approach that models sub-classes by storing and updating sub-prototypes, while keeping the CLIP backbone frozen. Here, CLIP is employed not for its zero-shot capability, but merely as a generic feature extractor. Fig. 3 illustrates the key differences between prior works and our approach. Unlike previous methods, and as motivated by Fig. 1, we reformulate UniDA as the simpler task of discovering target-private class names with generative VLMs. Specifically, we generate candidate labels directly from target-domain samples using a generative VLM, and then apply a filtering strategy that exploits image–text similarity to refine them.

2.3. *Out-Of-Distribution Detection*

Out-of-distribution (OOD) detection aims to identify samples during testing that come from distributions not encountered in training. Many research (Ming et al., 2022; Wang et al., 2023) leveraged vision-language foundation models, which integrate both visual and textual information to enhance the performance and flexibility of OOD detection. On the other hand, there is a sub-task of OOD detection known as Open-set recognition (OSR). OSR addresses the issue of OOD detection at a class level and is even more closely related to UniDA. Scheirer et al. (2012) first articulated the concept of OSR, which has since inspired extensive research across various fields (Bendale and Boult, 2016; Ge et al., 2017; Oza and Patel, 2019; Vaze et al., 2022; Esmaeilpour et al., 2022; Cen et al., 2023).

Among these, the recent study aims to leverage CLIP's zero-shot capability for open-set domain adaptation (Zara et al., 2023). However, there are significant limitations when applying this method (Zara et al., 2023) directly to UniDA. The number of clusters, K, is determined based on prior knowledge from the open-set, where the number of clusters exceeds the number of source labels. In a universal set, the decision of K is more challenging as its extent is not pre-defined. Specifically, when using K-means to predict the number of classes, the elbow method is typically applied (Hartigan and Wong, 1979). However, the elbow point is often unreliable due to a smooth score plot, leading to inaccuracies. Furthermore, we argue that texts discovered from the source domain are ineffective for detecting target private classes due to domain shifts, as the shapes of objects can differ entirely between the source and target domains, especially for abstract labels.

Unlike previous methods, our approach leverages instance-level discovery by comparing each discovered label with source labels based on image-text similarity. This eliminates the need to predefine the number of clusters, which would otherwise depend on the specific configurations of datasets. Also, we propose discovering target private classes by examining the rela-

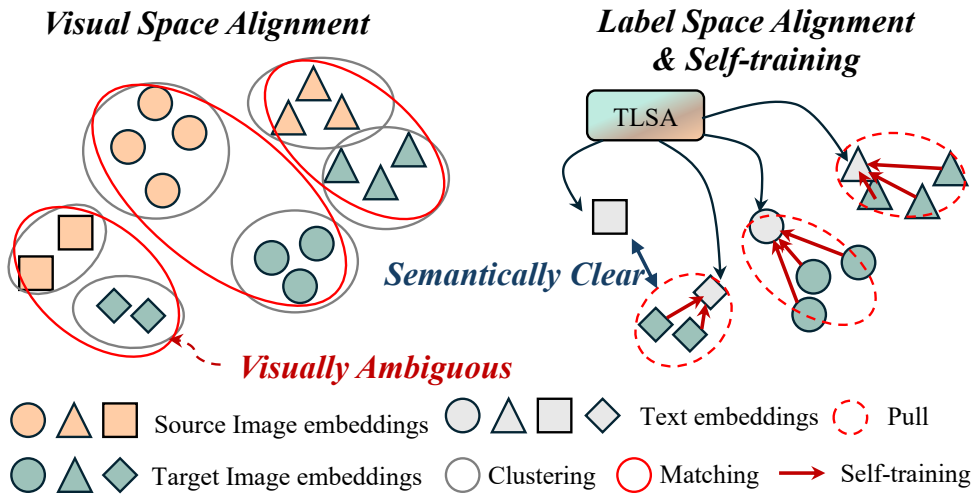

Figure 3: Comparison between existing UniDA methods and our proposed TLSA. Left: Prototype-based methods (Li et al., 2021a; Chang et al., 2022; Lai et al., 2023) construct target prototypes but struggle with visually. Right: Our TLSA identifies target private labels using only source labels and target samples.

tionship between an unbiased text representation and only the target image representation.

2.4. Self-Training

Self-training is a widely studied approach in semi-supervised learning that has recently been explored for enhancing the performance of minority classes (Amini et al., 2024). In situations where domain shift exists, research has primarily focused on Source-free domain adaptation (SFDA) and Test time adaptation (TTA). One of the most well-known approaches is a pseudo labeling technique, which is both simple to implement and intuitive. Pseudo labeling assumes that predictions for confident samples are trustworthy. Initially, training leverages these trustworthy predictions, and as the model advances, the scope of pseudo labeling is progressively broadened. The most important aspect is to maintain class balance. Class imbalance can lead to overconfidence in certain classes, which ultimately degrades the model's performance. To mitigate this issue, various source-free domain adaptation methods, such as SHOT (Liang et al., 2020) and DIFO (Tang et al., 2024) incorporate a diversity term to perform entropy maximization. ST-SGG (Kim et al., 2024) devises a method to adapt class-adaptive thresholds based on frequency, adjusting them according to the situation in previous iterations.

Inspired by this research direction, we choose to select the top-k most confident samples for each predicted class as pseudo labels to ensure class balance. Furthermore, to maintain this balance among the pseudo labels, we define k as the batch size divided by the number of predicted classes. This approach limits the selection to samples that can be easily classified. Additionally, we empirically confirm that our universal classifier, created by predicted target private labels, discriminates better than the $|C_s|$+1 way classifier, where $|C_s|$ is the number of source classes (Fig. 7).

3. Methodology

3.1. Problem Definition

In UniDA, there is a labeled source domain $\mathcal{D}^s = \{(x_i^s, y_i^s)\}_{i=1}^{N_s}$ where $x_i^s \in \mathcal{X}^s, y_i^s \in \mathcal{Y}^s \subset \mathbb{R}^{|C_s|}$, and an unlabeled target domain $\mathcal{D}^t = \{x_j^t\}_{j=1}^{N_t}$ where $x_j^t \in \mathcal{X}^t$. We denote the ground-truth labels of the target domain as $\mathcal{Y}^t \subset \mathbb{R}^{|C_t|}$. $|C_s|$ represents the number of source labels, and $|C_t|$ represents the number of target labels. $C = C_s \cap C_t$ denotes the common label sets shared by source and target domains. $\bar{C}_s = C_s - C$ and $\bar{C}_t = C_t - C$ stand for source-private label and target private label, respectively. Our goal is to filter the raw discovered label R from the generative VLM to align the ground-truth target private classes $\bar{C}_t$.

3.2. Overview

We verified that selecting target private labels derived from discovered labels substantially boosted performance under domain and label space shifts, as displayed in Fig. 1. We introduce TLSA, which iteratively aligns ambiguously similar labels with source labels from the discovered labels and ultimately filters them based on their occurrence patterns after all iterations. Following the TLSA pipeline, we employ a self-training strategy to further enhance discrimination and performance. The overall framework is depicted in Fig. 4.

• *Step 1.* The goal of this step is to filter the discovered labels by explicitly identifying and removing lexical synonyms of source labels using the WordNet database (Section. 3.3 and Fig. 4a).

• *Step 2.* The objective of this step is to remove discovered labels that are semantically ambiguous or resemble the source labels by identifying a similar label set in CLIP's joint embedding space (Section 3.4 and Fig. 4b).

We iterate *Step 1* and *Step 2* in each cycle until the entire domain is comprehensively explored. We define the refined label set as target private candidate labels.

• *Step 3.* To address rare instances missed in the previous phase,

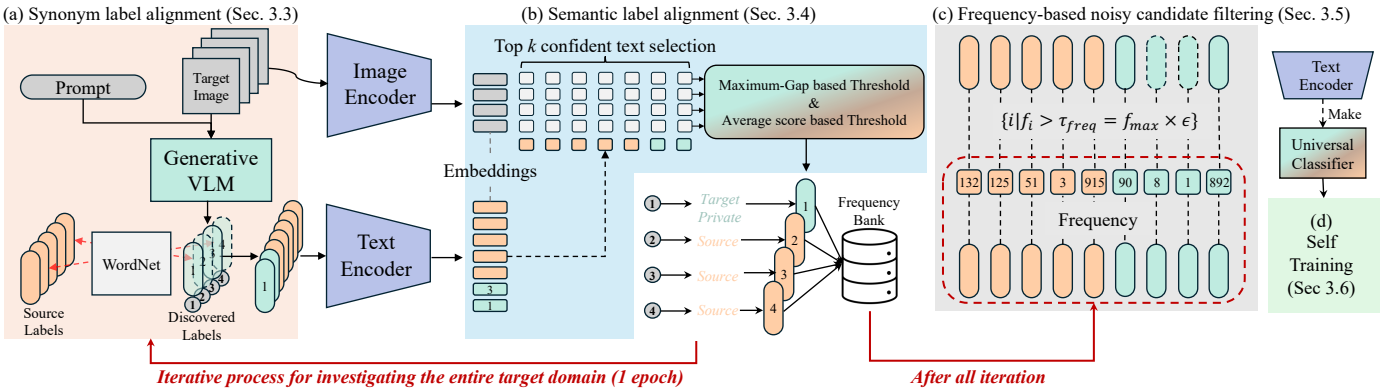

Figure 4: Overview of TLSA. We first gather candidate target-private labels from a generative VLM, then refine them to train a universal classifier. (a) Synonym alignment (Section 3.3) removes source label synonyms via WordNet: (b) Semantic alignment (Section 3.4) re-scores image-label pairs in the embedding space and decides shared vs. target-private; (c) Frequency filtering (Section 3.5) prunes noisy low support candidates using frequency banks; (d) Self-training (Section 3.6) applies a teacher-student scheme on class-balanced top-k confident samples.

we removed labels based on their occurrence frequency, operating under the assumption that infrequent target private candidate labels were likely incorrect target private labels (Section 3.5 and Fig. 4c).

• *Step 4.* This step aims to fully adapt the zero-shot model to the target domain, thereby enhancing its performance beyond zero-shot inference. This enhancement is achieved by utilizing a universal classifier weighted by CLIP text embeddings (Section 3.6 and Fig. 4d).

3.3. Synonym Label Alignment

In this subsection, we introduce a method for generating raw labels and eliminating synonyms. To acquire the discovered labels, we employ a generative VLM to generate labels for unknown target images. Furthermore, we use WordNet (Miller et al., 1990) to remove semantically ambiguous labels (i.e., synonyms) from the discovered labels, ensuring their alignment with the source label space, as illustrated in Fig. 4(a).

Discovering labels on unlabeled target images. To ensure reliable labels for the input images, we query each target sample x_i^t using the BLIP-VQA model (Li et al., 2022, 2023). Specifically, we utilize $k = 5$ prompts that are semantically equivalent yet lexically diverse, as presented in Table 14. The design of these prompts is informed by the principles of prompt engineering in CLIP (Radford et al., 2021), employing multiple textual variants to reduce prompt sensitivity. Consider prompts like "What is the exact name of the object in the painting?" and "Identify the object in this photo with its exact name," which share identical semantics but vary in phrasing. If the model's response was overly specific (e.g., detailing a color) or did not correspond to a single valid label, we omitted it from subsequent majority voting. We determined the final discovered label by applying majority voting across k responses. Although a comprehensive ablation study across different k values was not performed, preliminary observations suggested that $k = 5$ struck a balance between computational efficiency and stability; hence, we consistently employed this setting throughout our experiments.

Synonym label alignment using WordNet. WordNet (Miller et al., 1990) is a widely utilized lexical database that provides taxonomic relationships among words. Path-based similarity measures are computed by assessing the distances between two synsets within the hierarchy. Previous studies have applied WordNet to visual recognition (Ge et al., 2023) to explore parent–child relationships between labels. Additionally, WordNet can discern different lexical forms of a word, aiding in identifying synonymous relationships. Consequently, we employed WordNet as an essential filtering step to eliminate noisy labels in R.

3.4. Semantic Label Alignment

In this subsection, we detail the removal of hypernyms, hyponyms, incorrect (noisy) labels of the source class, and synonyms not present in the WordNet database. We employed semantic similarity to evaluate the relationship between the text representations of the source and candidate labels, based on their embedding distances from the input images. If candidate labels have a similar proximity to the image as the source labels, they are deemed identical to the corresponding source label, as displayed in Fig. 4b.

Leveraging Semantic Text-Image Similarity. Initially, text is converted into semantic embeddings to enable a more precise evaluation of image-text similarity. The filtered discovered labels $\tilde{R}$ are encoded as $\mathbf{z}_{\tilde{R}} = f_t(\tilde{R})$ using the text encoder f_t of CLIP, and subsequently augmented with the source class embeddings $\mathbf{z}_{C_s} = f_t(C_s)$. We assess the similarity between the augmented embedding $\mathbf{z_t} = [\mathbf{z}_{C_s}, \mathbf{z}_{\tilde{R}}]$, which comprises the source labels $\mathbf{z}_{C_s}$ and the filtered discovered labels $\tilde{R}$, and the image embedding $\mathbf{z}_v = f_v(X^t)$ produced by CLIP's visual encoder f_v. This evaluation determines whether the sample belongs to the target private classes or to the shared classes. The similarity score $S = sim(\mathbf{z}_v, \mathbf{z}_t)$ indicates if a text is source-related, where $sim(\cdot, \cdot)$ represents a cosine similarity function.

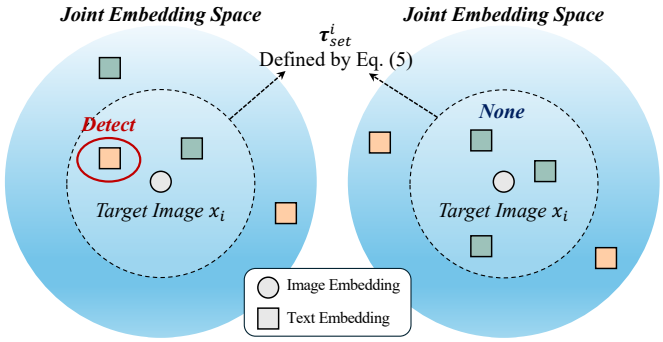

(a) Target Image x_i is considered to *source label*. (b) Target Image x_i is considered to *target private label*.

Figure 5: Illustration of semantic label alignment. In this step, we establish the relationship between discovered labels and source label predictions within the prediction set C, as defined by Eq. 5, for a given image x_i. (a) When source labels are present in C, the input image is classified as belonging to one of the source classes. (b) When no source labels exist in C, the input image is categorized as a target private class. Subsequently, we maintain a frequency count of classes in the frequency bank to enable noisy candidate filtering.

S is defined by Eq. 1.

$$\mathbf{s} = \begin{pmatrix} s_{1,1} & \cdots & s_{1,|C_s|} & s_{1,|C_s|+1} & \cdots & s_{1,|\tilde{R}|} \\ \vdots & \ddots & \vdots & \vdots & \ddots & \vdots \\ s_{N,1} & \cdots & s_{N,|C_s|} & s_{N,|C_s|+1} & \cdots & s_{N,|\tilde{R}|} \end{pmatrix} \tag{1}$$

where N denotes the batch size. The left part of S indicates the cosine similarity between the image embeddings and the source label embeddings, whereas the right part corresponds to the cosine similarity between the image embeddings and the filtered discovered label embeddings.

Identification of Target Private Labels from Filtered Discovered Labels. Using semantic similarity, we aim to determine whether an input image belongs to the source or target private classes. An overview of this procedure is presented in Fig. 5. When determining whether a label originates from a source private or target, we found that naive alignment methods—such as top-1 prediction-based alignment and margin-based alignment—performed poorly in our experiments (see Table 8). For instance, when 'backpack' is the source label and 'bag' is the discovered label (Fig. 2c), 'bag' and 'backpack' are not synonyms in WordNet; however, within the Office31 context, they effectively represent the same class. Treating them as distinct categories leads to numerous 'backpack' samples being misclassified as 'bag,' resulting in artificial label splits. In such cases, top-1 predictions may alternate between 'backpack' and 'bag' due to uncontrollable image conditions, without signifying any meaningful semantic difference. These semantically ambiguous labels might be included among certain target private labels. To address this, the margin score between the top-1 and top-2 predictions can evaluate the distance between source labels and the filtered discovered labels. However, this method relies on a predefined fixed threshold to assess reliability, ignoring class similarities that may vary adaptively across datasets and domains.

To overcome this limitation, we adaptively align the filtered discovered labels with source labels, removing the need for a fixed threshold. By analyzing the similarity matrix S, we first eliminate noisy labels and identify only reliable predictions within the top k predictions. We define a prediction set C as the collection of refined and filtered predictions from the top k predictions using the two proposed criteria.

• *Criterion 1. (Maximum-gap-based thresholding)* A prominent gap in similarity scores was identified among the top k rankings. The labels preceding this gap accurately correspond to multiple image predictions. Utilizing this criterion, we establish the meaningful prediction set C. The threshold is defined as follows:

$$J = \underset{j\in\{1,\ldots,k-1\}}{\arg\max} \left(s_{i,j-1} - s_{i,j}\right), \tag{2}$$

$$\tau^i_{\text{gap}} = s_{i,J}, \tag{3}$$

where i represents the image index, j the ranking position, and J denotes the point at which a significant gap occurs.

• *Criterion 2. (Average score-based thresholding)* Similarly, we define the prediction set as comprising scores that exceed the average score of the top k predictions. The subsequent equation specifies the threshold based on the average of the top k scores.

$$\tau^i_{avg} = \frac{\sum_{j=1}^{k} s_{i,j}}{k}. \tag{4}$$

Empirically, we maximize the prediction set size by selecting the lower of the two criteria. This approach enhances the inclusion of source labels within the label set, thereby reducing the likelihood of ambiguous labels being identified as private target candidates. In other words, by selecting the smaller threshold between τ_{gap} and τ_{avg}, the criterion for classifying a sample as target private becomes more stringent. The threshold τ_{set} and prediction set C for each instance are formulated as follows:

$$\tau^i_{set} = \min(\tau^i_{gap}, \tau^i_{avg}), \tag{5}$$

$$C^i = \{\mathbf{t}_{i,j} | j \in I^i_k \wedge s_{i,j} > \tau^i_{set}\}, \tag{6}$$

where $\mathbf{t}$ represents the text comprising extensions of source labels and filtered discovered labels, and I^i_k denotes the top-k indices for the i^{th} sample. Utilizing the selected prediction set C, we perform a source label presence check to achieve semantic label alignment. Specifically, if a source label is present in C^i (Fig. 5a, sample i is classified as a source sample. When it is absent from the prediction set C, sample i is identified as a target private sample (Fig. 5b).

3.5. Frequency-based Noisy Candidate Filtering

Noisy and incorrectly predicted private target candidate labels may still persist. To address this, we developed a method that filters these noisy labels by analyzing their frequencies, as shown in Fig. 4 (c). We hypothesized that low-frequency classes are likely noisy labels in the target domain. To precisely measure label frequency, we employed a frequency bank. For samples classified as source classes, the top-1 prediction $p_i$was stored in the frequency bank as a reference standard (Fig. 5a). Similarly, for samples classified as target private classes, the discovered label $r_i$is added to the frequency bank

even if $r_i \notin C^i$(Fig. 5b). The rationale for storing r_i, the label identified by BLIP, instead of p_i, the closest label in the CLIP space, is detailed in Appendix 11. The frequency bank is defined as $F = \{c : f_c\}$, where f_c represents the frequency of class c after semantic label alignment, including both source and filtered discovered labels. Considering the presence of noisy labels in the frequency bank, we used the count of the most frequent class rather than the median or mean of the label frequency distribution. We set a threshold τ_{freq}as the fixed number of samples in the most frequent class. This scaling factor, denoted by ϵ, is a dataset-agnostic parameter. Finally, the predicted target private labels C_p are derived from the raw discovered labels R as follows:

$$\tau_{freq} = \epsilon \times \max(F), \tag{7}$$

$$C_p = \{c | f_c > \tau_{freq} \wedge c \notin C_s\}. \tag{8}$$

We employ an empirically determined value of $\epsilon = 0.01$ across all datasets, as presented in Table 10.

By integrating complementary signals—lexical similarity validated with WordNet, semantic similarity calculated within a joint image–text embedding space, and a final statistical test that eliminates residual noisy discovered labels—our pipeline outperforms naïve filtering significantly, as demonstrated in Table 7.

3.6. Self-Training with Universal Classifier

In UniDA, the prior typically uses randomly initialized prototype-based classifiers (Li et al., 2021a; Chang et al., 2022; Lai et al., 2023). However, this method complicates determining the number of target clusters, which corresponds to the number of private target classes. In contrast, we utilize a universal classifier that automatically determines the number of target private classes, as depicted in Fig. 4d. Furthermore, we applied self-training, a prevalent technique in source-free domain adaptation Liang et al. (2020); Zhang et al. (2023); Karim et al. (2023); Tang et al. (2024). This method reduces bias toward the source domain, offering an advantage over approaches that depend on visual-space domain alignment and source-supervised learning. Additionally, we selected reliable pseudo-labels based on the top-k confidence samples per class and employed a student-teacher framework with EMA updates.

Creating a Universal Classifier. Our inference leverages the weights of the *universal classifier*, denoted by $\mathbf{z}_{C_s}$ and $\mathbf{z}_{C_p}$, which are produced by inputting C_p into the text encoder of CLIP. For post-processing, instances classified as C_s were retained unchanged, while those labeled as C_p were adjusted to $|C_s| + 1$, ensuring a threshold-free method.

Reliable Pseudo Label Selection and Self-Training. To leverage pseudo-labels, we trained a student model to enhance the teacher model's performance using delayed updates. However, naive pseudo-labeling tends to select only easily classifiable classes, leading to overfitting of these simpler categories. To address this, we introduce a balanced pseudo-label selection strategy that improves the generalization of the predictions of the pretrained model. Rather than requiring a large dataset, our approach prioritizes maximum diversity by selecting the top-k% most confident pseudo-labels per class, as proposed by Zara et al. (2023). Nonetheless, even with a top-k% threshold, more prevalent classes are disproportionately selected, which can degrade performance. To mitigate this, we define a balanced k value to select only the top-k most confident samples for each class. Specifically, k is calculated as $k = \min\{n_{c_i}, N/n_c\}$, where n_c is the number of unique predicted classes and n_{c_i} is the number of predictions for class c_i.

Table 1: Split-setting of our experiments. (Source Private / Shared)

Datasets	Split settings			
	open-partial	open	closed	partial
Office31	10/10	0/10	0/31	21/10
Office-Home	5/10	0/15	0/65	40/25
VisDA	3/6	0/6	0/12	6/6
DomainNet	50/150	0/150	0/345	195/150

To ensure robust self-training, we apply Exponential Moving Average (EMA) updates to the teacher model, defined by $\theta_t = (1 - \alpha)\theta_s + \alpha\theta_t$. Here, θ_t and θ_s represent the parameters of the teacher and student models, respectively, effectively mitigating confirmation bias. The student model updates with each iteration, whereas the teacher model updates once per epoch, as defined by the preceding equation. This configuration is crucial for the performance of the model (Section 5). Additionally, we implemented adapter tuning to limit further tuning capabilities.

Consequently, we performed self-training using the following loss function: Let M represent the set of samples employed as pseudo-labels, $\hat{y}^T_{t,i}$denotes the output of the teacher model, and $\hat{y}^S_{t,i}$represents the output of the student model.

$$\mathcal{L}_{self} = -\sum_{i \in M} \hat{y}^T_{t,i} \log \hat{y}^S_{t,i}, \tag{9}$$

By utilizing a frozen classifier, a common approach in SFDA (Liang et al., 2020), adapter tuning mitigates error accumulation by addressing the delayed conversion rate.

4. Experiments

This section outlines the dataset, implementation, experimental settings, and results.

Datasets. We utilize four benchmark datasets for visual recognition domain adaptation: Office31 (O), Office-Home (OH), VisDA (VD), and DomainNet (DN). Office31 (Saenko et al., 2010) is a small-scale benchmark dataset comprising images from 31 categories distributed across three domains: **A**mazon (2,817 images), **D**slr (498 images), and **W**ebcam (795 images). Office-Home (Venkateswara et al., 2017) is a benchmark dataset designed for domain adaptation, featuring images from 65 categories across four domains: **Ar**t (9,655 images), **Cl**ipart (9,516 images), **Pr**oduct (15,688 images), and **R**eal**w**orld (14,840 images). VisDA (Peng et al., 2017) is

a benchmark dataset for domain adaptation, containing images from 12 labels distributed across two domains: **Syn**thetic (152,397 images) and **Real** (55,088 images). DomainNet (Peng et al., 2019) is a large-scale benchmark dataset for domain adaptation, notable for its extensive size. It includes images from 345 labels distributed across six domains: **Clipart**, **Infograph**, **Painting**, **QuickDraw**, **Real**, and **Sketch**. The sheer scale of DomainNet makes it a particularly challenging and comprehensive dataset for evaluating domain adaptation methods. We conducted experiments using only three domains from DomainNet that are commonly employed in existing methods for UniDA - Painting, Sketch, and Real.

Baselines. This section lists the baseline methods we used for comparison. Most of the performance results are referenced from GLC++(Qu et al., 2024c), MLNet(Lu et al., 2024), MemSPM (Lai et al., 2023), and LEAD (Qu et al., 2024b). The lists below are the ones that link to their respective references: Source-only(SO), DANCE[a] (Saito et al., 2020), OVANet[b] (Saito and Saenko, 2021), UniOT[d] (Chang et al., 2022), WiSE-FT[e] (Wortsman et al., 2022), CLIP-Distill[e] (Deng and Jia, 2023), GLC[f] (Qu et al., 2023b), MemSPM[g] (Lai et al., 2023), UAN[h] (You et al., 2019b), CMU[i] (Fu et al., 2020), DCC[j] (Li et al., 2021a), GATE[k] (Chen et al., 2022a), MLNet[l] (Lu et al., 2024), LEAD[m] (Qu et al., 2024b).

Implementation details. We use CLIP (Radford et al., 2021) backbone with ViT-B/16 (Dosovitskiy et al., 2020) as our image encoder. For the generative VLM, we utilize BLIP (Li et al., 2022), a model pretrained on VQAv2 (Goyal et al., 2017) within the LAVIS library[1]. This model incorporates a visual encoder based on ViT-Base (Dosovitskiy et al., 2020) and employs a text encoder and decoder that adhere to the BERT (Devlin et al., 2018) architecture. Most of the baseline code and pipelines are based on the uniood repository[2].

During the alignment phase, to expedite filtering, we conducted experiments with a batch size of 128. These experiments were executed on a single H100 GPU, consuming approximately 15GB of memory during the filtering process. As the source domain was not trained separately, the overall experimental time was significantly reduced.

In the self-training phase, we conducted experiments with a batch size of 64, a learning rate of 0.01, and an adapter with bottleneck dimensions of r=64, adhering to the default settings of AdaptFormer (Chen et al., 2022b). All baseline methods were implemented with identical iterations, batch sizes, and learning rates using a frozen backbone, as described in Deng and Jia (2023). The iterations were set to 2,500; 5,000; and 10,000, depending on the task setting, as presented in Table 2, following (Deng and Jia, 2023). Our methods required approximately 30 min per domain, allowing us to complete all experiments on the entire dataset within a day.

[1] https://github.com/salesforce/LAVIS

[2] https://github.com/szubing/uniood

Table 2: Training iterations on different split settings. We follow the same setting in (Deng and Jia, 2023). Since we use batch size 64, which is twice the original value, we reduce the number of iterations accordingly by half.

Datasets	Split settings			
	open-partial	open	closed	partial
Office31	2500	2500	5000	5000
Office-Home	2500	2500	5000	5000
VisDA	5000	5000	10000	10000
DomainNet	5000	5000	10000	10000

Evaluation metric. We use the existing two evaluation metrics for UniDA in addition to classification accuracy. H-score (Fu et al., 2020) is the harmonic mean of the instance accuracy on common class a_C and accuracy on the single private class $a_{\bar{C}_t}$. This metric effectively captures the trade-off between known-class accuracy and out-of-class detection accuracy. Moreover, we also use the H^3-score. The H^3-score is first proposed by UniOT (Chang et al., 2022) and extends the H-Score by incorporating the Normalized Mutual Information (NMI), a well-known measure that indicates how well the target private clusters are formed. In the PDA and CDA settings where target private instances do not exist, the average class accuracy is used in place of the H-score. Similarly, the H^3 score is also substituted with this measure.

5. Results

5.1. Quantitative Comparison

Comparison with baseline methods. We compared TLSA against existing UniDA approaches. Among these, CLIP-Distillation achieves state-of-the-art (SOTA) performance. Except for the Office31 open-set and VisDA partial settings, we attain SOTA across all scenarios. Although the impact of self-training is more significant on certain datasets, it generally enhances the H^3-score in most cases. The results are summarized in Table 3. Since calculating the H-score and H^3-score for partial and closed-set scenarios is infeasible, we employed the average accuracy score as a substitute for the H-score and H^3-score, following Deng and Jia (2023). These findings highlight the versatility and effectiveness of TLSA and TLSA+ST (Self-Training) across diverse UniDA settings, particularly in open-partial and open scenarios where managing unseen classes is critical.

In the open-partial setting, TLSA+ST achieved the highest scores across datasets, with H-scores of 93.5 for Office-Home and 87.3 for VisDA. The H^3-scores were similarly high, reaching 89.2 on Office-Home and 87.6 on VisDA, demonstrating the ability of TLSA+ST to adapt to partially overlapping classes. In the open setting, TLSA+ST leads with H-scores of 95.2 on Office31 and 87.6 on VisDA, while H^3-scores are also competitive at 89.9 on Office31 and 84.9 on VisDA, showcasing the robustness of the method in managing unseen target classes. In the closed setting, where all classes overlap, TLSA+ST maintained competitive performance with an H-score of 75.6 on VisDA,

Table 3: H-score (%) and H^3-score (%) comparisons between existing methods and the proposed method using the CLIP ViT-B/16 backbone across four UniDA settings (open-partial, open, closed, partial). An asterisk (*) represents results for some methods referenced from the previous paper Lai et al. (2023). A dash (-) represents that any metrics not reported in the official papers.

Methods	Office31				Office-Home				VisDA				DomainNet				Avg
	(10/10)	(10/0)	(10/21)	(31/0)	(10/5)	(15/0)	(25/40)	(65/0)	(6/3)	(6/0)	(6/6)	(12/0)	(150/50)	(150/0)	(150/195)	(345/0)	
H-score																	
SO	85.8	86.8	83.8	70.8	79.1	76.5	51.8	49.6	67.8	71.4	49.1	51.1	55.8	59.7	32.9	34.8	62.9
DANCE	91.7	93.2	73.8	67.7	83.6	78.3	46.9	49.4	66.6	76.6	33.7	46.3	55.1	59.4	30.0	34.1	61.6
OVANet	89.0	89.3	84.0	65.9	80.5	76.3	58.8	56.1	56.6	44.4	36.6	40.9	62.0	64.4	45.0	46.2	62.2
UniOT	82.3	93.9	31.5	54.2	86.3	81.8	31.8	46.4	58.2	77.3	33.6	54.2	65.6	69.4	40.9	51.5	59.8
WiSE-FT	70.4	88.3	38.5	30.9	72.8	65.8	11.7	8.8	54.7	67.8	19.1	22.2	2.4	6.0	0.19	0.2	35.0
CLIP-Distill	83.5	84.3	85.6	73.7	84.7	81.3	74.4	69.0	82.8	82.2	78.7	71.1	64.8	66.7	56.4	51.3	74.4
GLC*	84.8	90.1	91.5	-	82.6	86.2	75.4	-	80.3	81.6	86.2	-	46.8	-	-	-	-
MemSPM*	88.5	**95.6**	94.4	-	84.2	87.9	74.5	-	79.3	79.7	**87.9**	-	56.7	-	-	-	-
TLSA	89.9	92.6	96.1	80.5	91.3	89.2	82.0	79.0	86.3	83.9	81.8	72.6	**75.4**	**76.9**	70.1	**68.9**	82.3
TLSA+ST	**91.9**	95.2	**96.9**	**82.9**	**93.5**	**91.4**	**85.3**	**81.8**	87.6	**86.0**	83.0	**75.6**	74.3	74.9	**74.4**	67.9	**83.9**
H^3-score																	
SO	83.4	85.8	83.8	70.8	77.2	75.2	51.8	49.6	72.6	73.4	49.1	51.1	59.6	62.5	32.9	34.8	63.3
DANCE	87.0	89.8	73.8	67.7	80.5	77.7	46.9	49.4	71.7	76.9	33.7	46.3	59.1	62.2	30.0	34.1	61.6
OVANet	85.2	87.3	84.0	65.9	78.0	75.2	58.8	56.1	63.6	51.8	36.6	40.9	64.1	65.8	45.0	46.2	62.8
UniOT	80.7	89.8	31.5	54.2	82.3	79.7	31.8	46.4	61.3	75.8	34.0	53.6	66.6	69.0	40.9	51.5	59.3
WiSE-FT	72.5	86.6	38.5	30.9	72.0	68.1	11.7	8.8	71.5	78.3	19.1	22.2	3.6	8.6	0.2	0.2	37.1
CLIP-Distill	81.7	83.8	85.6	73.7	80.2	78.3	74.4	69.0	81.8	86.0	78.7	71.1	66.1	67.4	56.4	51.3	74.1
TLSA	**85.8**	89.1	96.1	80.5	84.8	82.9	82.0	79.0	85.7	81.7	81.8	72.6	73.0	73.9	69.6	**68.2**	80.5
TLSA+ST	85.3	**89.9**	**96.9**	**82.9**	**90.2**	**89.0**	**85.3**	**81.8**	**88.4**	**85.0**	**83.0**	**75.6**	**75.4**	**75.5**	**74.4**	67.9	**83.2**

significantly surpassing other methods. In the partial setting, TLSA+ST also delivered strong results, achieving an H-score of 74.4 on DomainNet. Collectively, these results highlight the effectiveness of TLSA and TLSA+ST across various UniDA scenarios, particularly excelling in open-partial and open settings where handling unseen classes is crucial.

Tables 4 and 5 compare our results with existing methods in the open partial domain adaptation scenario using both ResNet50 (ImageNet-pretrained) and ViT-B/16 (CLIP-pretrained) backbones. Our approach achieved state-of-the-art performance across nearly all domain-to-domain adaptations. However, a slight reduction in H-score was observed due to self-training in DomainNet. While closed-set accuracy improved, OOD detection performance tended to decrease, and vice versa. This indicates a trade-off: self-training shifts the focus of the model, often leading to a decline in H-score performance.

Robustness in various UniDA. We compared the performance of our TLSA method with existing approaches, including CLIP-distillation and UniOT, across different category splits. With a fixed number of shared labels, we designed five settings for $\bar{C}_s/C/\bar{C}_t$: 5/10/50, 20/10/35, 30/10/25, 40/10/15, and 50/10/5 for Office-Home, and three settings: 50/150/145, 100/150/95, and 150/150/45 for DomainNet. Fig. 6 demonstrates the robustness of our TLSA method to variations in these split settings.

5.2. Qualitative Comparison

Feature visualization. We present t-SNE (Long et al., 2016) plots in Fig. 7 to compare feature discrimination between the CLIP zero-shot and $|C_s|$ + 1classifiers using our approach. As other methods employ a fixed backbone identical to that in (Deng and Jia, 2023), we omitted their representations from the visualization. Furthermore, to emphasize our universal classifier's discriminative ability, we utilized a $|C_s|+1$classifier with LP-ST (linear probing via self-distillation and self-training using top-k confident sample selection), similar to LP-FT (Kumar et al., 2022). The $|C_s|$ + 1-way classifier underperforms compared to TLSA due to its constrained capacity to represent unknown classes.

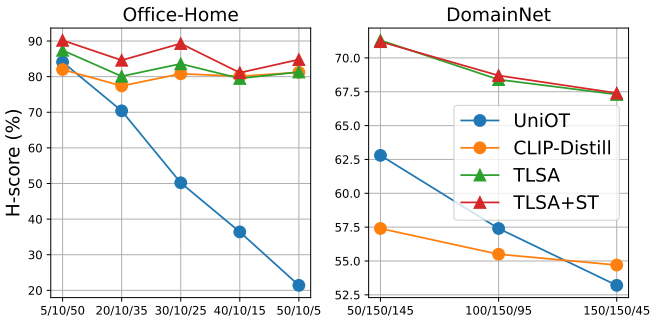

Figure 6: Robustness across different class split settings in Office-Home, Real-World to Clipart, and DomainNet Real to Painting.

Predicted target-private labels analysis. Table 6 presents examples of the target-private set extracted by the proposed method. We observed that these predicted labels align with the ground-truth target-private categories in the target domain under the DSLR setting of Office31, indicating that TLSA effectively identifies genuine target-private classes. Importantly, the discovered labels do not need to precisely match the ground-truth annotations; they may also capture prominent attributes of target-domain images. This flexibility is beneficial because generative VLMs can function effectively even on objects not encountered during pretraining, making them particularly

Table 4: H-score (%) comparison in OPDA scenarios on the Office-Home dataset. Results for some methods are referenced from GLC++ (Qu et al., 2024c) and LEAD (Qu et al., 2024b). Here, SF indicates source data-free methods, and SM denotes approaches that use a source model. We compare TLSA with both source-free methods and those using source models. An asterisk (*) indicates reproduced results.

Backbone	Methods	SF	SM	Office-Home												Avg
				Ar2Cl	**Ar2Pr**	**Ar2Re**	**Cl2Ar**	**Cl2Pr**	**Cl2Re**	**Pr2Ar**	**Pr2Cl**	**Pr2Re**	**Re2Ar**	**Re2Cl**	**Re2Pr**	
ImageNet	SO	✓	✓	47.3	71.6	81.9	51.5	57.2	69.4	56.0	40.3	76.6	61.4	44.2	73.5	60.9
	UAN[h]	✗	-	51.6	51.7	54.3	61.7	57.6	61.9	50.4	47.6	61.5	62.9	52.6	65.2	56.6
	CMU[i]	✗	-	56.0	56.9	59.2	67.0	64.3	67.8	54.7	51.1	66.4	68.2	57.9	69.7	61.6
	DANCE[a]	✗	-	61.0	60.4	64.9	65.7	58.8	61.8	73.1	61.2	66.6	67.7	62.4	63.7	63.9
	DCC[j]	✗	-	58.0	54.1	58.0	74.6	70.6	77.5	64.3	73.6	74.9	81.0	75.1	80.4	70.2
	GATE[k]	✗	-	63.8	75.9	81.4	74.0	72.1	79.8	74.7	70.3	82.7	79.1	71.5	81.7	75.6
	OVANet[b]	✗	-	61.7	77.3	80.6	68.9	68.7	61.9	50.4	47.6	61.5	62.9	52.6	65.2	56.6
	UniOT[c]	✗	-	67.3	80.5	86.0	73.5	77.3	84.3	75.5	63.3	86.0	77.8	65.4	81.9	76.6
	GLC[f]	✓	✓	64.3	78.2	89.8	63.1	81.7	89.1	77.6	54.2	88.9	80.7	54.2	85.9	75.6
	MLNet[l]	✗	-	68.2	83.8	85.0	73.6	78.2	82.2	75.2	64.7	85.1	78.8	69.9	83.9	77.4
	LEAD[m]	✓	-	62.7	78.1	86.4	70.6	76.3	83.4	75.3	60.6	86.2	75.4	60.7	83.7	75.0
CLIP	SO*	✓	✓	69.8	80.3	83.8	80.5	81.5	85.3	77.5	71.2	84.7	80.5	76.0	77.6	79.1
	DANCE*[a]	✗	-	78.0	86.4	87.1	81.1	85.2	85.6	82.4	79.9	90.5	83.6	79.6	84.1	83.6
	OVANet*[b]	✗	-	72.7	88.0	86.4	80.6	84.0	85.3	75.2	63.6	89.1	82.0	74.4	85.0	80.5
	UniOT*[c]	✗	-	85.5	89.8	91.1	79.9	87.3	89.3	80.8	83.5	88.9	83.5	84.3	91.6	86.3
	WiSE-FT*[d]	✓	✓	59.4	86.9	87.0	57.6	80.3	80.9	62.7	50.2	85.1	71.0	64.7	88.4	72.8
	GLC[f]	✓	✓	79.4	88.9	90.8	76.3	84.7	89.0	71.5	72.9	85.7	78.2	79.4	90.0	82.6
	DCC[j]	✗	-	62.6	88.7	87.4	63.3	68.5	79.3	67.9	63.8	82.4	70.7	69.8	87.5	74.4
	MemSPM[g]	✗	-	78.1	90.3	90.7	81.9	90.5	88.3	79.2	77.4	87.8	78.8	76.2	91.6	84.2
	CLIP-Distill*[e]	✓	✓	81.4	79.6	86.1	87.9	80.3	86.7	87.0	81.3	80.6	85.2	82.0	88.9	84.3
	TLSA	✓	✗	87.4	95.2	95.8	86.8	95.2	95.8	86.8	87.4	95.8	86.8	87.4	95.2	91.3
	TLSA+ST	✓	✗	**90.2**	**96.3**	**96.7**	**90.6**	**96.3**	**96.7**	**90.6**	**90.2**	**96.7**	**90.6**	**90.2**	**96.3**	**93.4**

Table 5: H-score (%) comparison in OPDA scenarios on the Office31, DomainNet, and VisDA datasets, respectively. MLNet (Lu et al., 2024) does not provide experimental results for DomainNet, any metrics not reported in their paper are marked as "-". An asterisk (*) indicates reproduced results.

Backbone	Methods	SF	SM	Office31							DomainNet							VisDA
				A2D	A2W	D2A	D2W	W2A	W2D	**Avg**	P2R	P2S	R2P	R2S	S2P	S2R	**Avg**	S2R
ImageNet	SO	✓	✓	70.9	63.2	39.6	77.3	52.2	86.4	64.9	57.3	38.2	47.8	38.4	32.2	48.2	43.7	25.7
	UAN[h]	✗	-	59.7	58.6	60.1	70.6	60.3	71.4	63.5	41.9	39.1	43.6	38.7	38.9	43.7	41.0	34.8
	CMU[i]	✗	-	68.1	67.3	71.4	79.3	72.2	80.4	73.1	50.8	45.1	52.2	45.6	44.8	51.0	48.3	32.9
	DANCE[a]	✗	-	78.6	71.5	79.9	91.4	72.2	87.9	80.3	21.0	37.0	47.3	46.7	27.7	21.0	33.5	42.8
	DCC[j]	✗	-	88.5	78.5	70.2	79.3	75.9	88.6	80.2	56.9	43.7	50.3	43.3	44.9	56.2	49.2	43.0
	GATE[k]	✗	-	87.7	81.6	84.2	94.8	83.4	94.1	87.6	57.4	48.7	52.8	47.6	49.5	56.3	52.1	56.4
	OVANet[b]	✗	-	85.8	79.4	80.1	95.4	84.0	94.3	86.5	56.0	47.1	51.7	44.9	47.4	57.2	50.7	53.1
	UniOT[c]	✗	-	83.7	85.3	71.4	91.2	70.9	90.8	82.2	59.3	47.8	51.8	46.8	48.3	58.3	52.0	57.3
	GLC[f]	✓	✓	81.5	84.5	89.8	90.4	88.4	92.3	87.8	63.3	50.5	54.9	50.9	49.6	61.3	55.1	73.1
	MLNet[l]	✗	-	83.9	78.5	81.3	95.4	83.2	96.4	86.5	-	-	-	-	-	-	-	69.9
	LEAD[m]	✓	✓	85.4	85.0	86.3	90.9	86.2	93.1	87.8	59.9	46.1	51.3	45.0	45.9	56.3	50.8	76.6
CLIP	SO*	✓	✓	84.4	79.0	88.1	93.3	80.2	89.8	85.8	64.2	50.2	53.1	52.1	48.3	67.1	55.8	67.8
	DANCE*[a]	✗	-	91.6	84.7	**93.7**	**95.8**	87.8	**96.4**	91.7	64.2	50.1	50.8	51.2	47.4	67.2	55.1	66.6
	OVANet*[b]	✗	-	86.8	76.1	90.1	94.9	91.0	95.2	89.0	68.2	58.6	60.5	59.1	57.0	68.6	62.0	56.6
	UniOT*[c]	✗	-	78.5	73.4	82.5	88.4	83.0	88.1	82.3	71.4	62.8	62.5	64.6	59.5	72.7	65.6	56.3
	WiSE-FT*[d]	✓	✓	60.4	50.7	72.6	77.9	70.6	90.2	70.4	5.07	1.15	2.84	1.64	0.84	3.06	2.43	46.5
	DCC[j]	✗	-	82.2	76.9	83.6	75.2	85.8	88.7	82.1	61.1	38.8	51.8	49.3	49.1	60.3	52.2	61.2
	GLC[f]	✓	✓	80.5	80.4	77.5	95.6	77.7	96.9	84.8	51.2	44.5	55.6	43.1	47.0	39.1	46.8	80.3
	MemSPM[g]	✗	-	88.0	84.6	88.7	87.6	87.9	94.3	88.5	62.4	52.8	58.5	53.3	50.4	62.6	56.7	79.3
	CLIP-Distill*[e]	✓	✓	81.6	81.1	87.7	81.0	87.6	81.8	83.5	74.2	61.6	58.5	60.2	59.7	74.8	64.8	81.9
	TLSA	✓	✗	92.7	86.8	90.1	86.8	90.1	92.6	89.9	**83.6**	**71.2**	**71.3**	**71.2**	**71.3**	**83.6**	**75.4**	86.3
	TLSA+ST	✓	✗	**95.4**	**88.7**	91.5	88.7	**91.5**	95.4	**91.9**	82.3	69.4	71.2	69.4	71.2	82.3	74.3	**87.6**

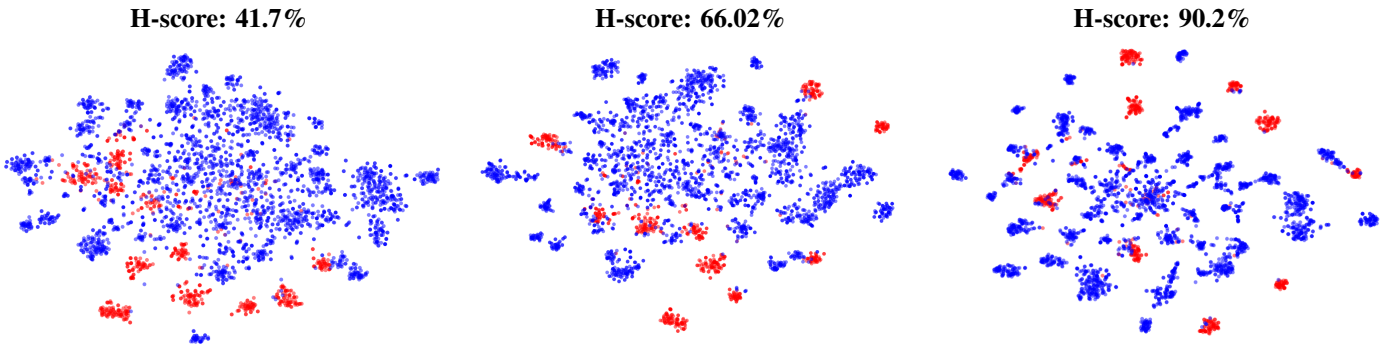

(a) CLIP zero-shot (b) TLSA+ST ($|C_s|$+1 classifier) (c) TLSA+ST (Universal classifier)

Figure 7: The t-SNE plots of target domain samples for the zero-shot and TLSA+ST methods in the Office-Home RealWorld→Clipart OPDA setting. Blue points indicate target-private samples, while red points represent source-class samples.

Table 6: List of ground truth target private labels and final candidates extracted from TLSA for the Office31, dslr, open-partial setting. The same color indicates the same semantic group.

True target private	Predicted target private	
pen	pen	bat
	pencil	-
printer	printer	fax machine
ruler	ruler	-
punchers	stapler	-
ring binder	fax machine	-
scissors	scissors	-
tape dispenser	paper dispenser	-
trash can	trash can	recycle bin
stapler	stapler	-
phone	modem	-
speaker	speaker	usb drive
-	tv	scale
	remote	

suited for open vocabulary or unknown classes. This process generates a set of discovered labels, $R = \{r_i\}_{i=1}^{N}$, where N represents the batch size of the target image.

Analysis of the number of predicted target private labels. Fig. 8 displays the number of predicted target-private labels in our study. Across various datasets and settings, our method accurately predicts target-private labels compared to their ground-truth counterparts. This illustrates the flexibility of our design in adapting to different split configurations and datasets.

5.3. Ablation Study

Ablation Study and Comparison of the Alignment Pipeline. We implement an ablation study of label space alignment. As can be seen in Table 7, Synonym label alignment serves as a fundamental filtering method, contributing to performance to a certain extent.

Top-1 prediction-based alignment relies solely on the top-1 prediction. If the top-1 prediction corresponds to a discovered label, the sample is classified as a target-private sample; otherwise, if it corresponds to a source label, it is identified as a shared sample. In contrast, margin-based alignment requires that, even when a discovered label is the top-1 prediction, it is considered a target-private candidate only if its score exceeds that of the top-1 source label by a specified margin. This margin is empirically fixed at $\frac{1}{|C_s|}$ across all instances, which yields the best performance for this method.

Frequency-based noisy candidate filtering is a vital component of our pipeline; without it, highly noisy candidate labels could be incorrectly designated as target-private labels. A comparison of these methods is shown in Table 7.

Ablation Study of Two Criteria for Label Space Alignment. We conducted an ablation study on the two thresholds, $\tau_{\text{avg}}$and τ_{gap}, used in adaptive filtering. As outlined in Table 8, τ_{avg}significantly impacts performance more than τ_{gap}. Furthermore, $\tau_{\text{avg}}$and τ_{gap}operate as complementary thresholds. Our design ensures robustness against split-setting variations and diverse datasets.

Ablation Study of Self-Training Components. We conducted experiments to enhance the reliability of our self-training design. The key observation was that incorporating delayed EMA components (Delay in Table 9) slowed the training process of the teacher model and significantly improved the model performance. Moreover, our approach surpassed the top-k% pseudo-label sampling strategy proposed in a previous study (Zara et al., 2023) (Table 9).

5.4. Further Analysis

This section includes sensitivity analyses of hyperparameters during the alignment process, scalability evaluations relative to backbone size, learning dynamics during self-training, and analyses of trade-offs related to source sample usage.

Sensitivity Analysis for Hyperparameters in TLSA. We analyze the sensitivity of our hyperparameters, k, in the top-k prediction within the label-space alignment pipeline and ϵ in frequency-based noisy candidate filtering. The results are presented in Table 10. The experiments on the DomainNet dataset determined the optimal value based on average performance.

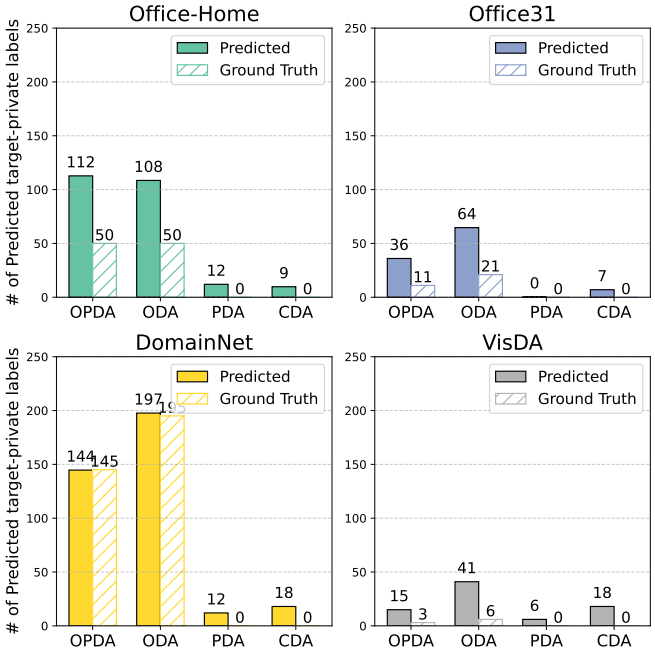

Figure 8: The number of predicted target private labels through change of split settings and datasets.

Table 7: Ablation study with different components of our alignment pipeline approach. The semantic alignment strategy refers to the comparison of alignment methods used in step 2. Top-1 refers to top-1 prediction-based alignment, Margin refers to margin-based alignment, and Align refers to our method.

Step 1	**Step 2**			**Step 3**	**Office31**				**Office-Home**				**VisDA**				**DomainNet**			
–	Top-1	Margin	Ours	–	OPDA	ODA	PDA	CDA	OPDA	ODA	PDA	CDA	OPDA	ODA	PDA	CDA	OPDA	ODA	PDA	CDA
✓	✓			✓	88.8	91.5	89.9	71.3	86.6	83.8	72.7	66.3	76.6	75.2	64.7	54.1	74.8	75.8	66.2	65.3
✓		✓		✓	89.2	92.1	91.6	71.7	87.3	84.5	72.9	66.4	77.8	77.4	67.2	57.2	75.1	76.1	66.6	65.5
			✓	✓	88.6	92.0	92.3	76.8	87.2	86.4	76.9	72.2	86.3	82.2	75.6	70.8	**76.1**	**77.1**	69.1	67.6
✓			✓		**90.0**	91.9	94.6	78.6	89.8	85.2	79.7	74.2	47.3	45.7	28.9	28.8	71.6	71.1	62.8	60.4
✓			✓	✓	89.9	**92.6**	**96.1**	**80.5**	**91.3**	**89.2**	**82.0**	**79.0**	**86.3**	**83.9**	**81.8**	**72.6**	75.4	76.9	**70.1**	**68.9**

Table 8: Ablation study comparing H-scores across different prediction set decision thresholds.

methods	OPDA	ODA	PDA	CDA	Avg
w/o τ_{gap}	**85.8**	**85.6**	81.0	75.0	81.9
w/o τ_{mean}	84.1	83.7	77.5	71.2	79.1
Ours	85.7	**85.6**	**82.5**	**75.2**	**82.3**

Specifically, we performed a sensitivity analysis on the k value used for top-k predictions in Step 2 (semantic label alignment) of the filtering pipeline. Our pipeline consistently outperformed other UniDA methods, leading us to select $k = 5$ for its robustness across various configurations.

We perform a sensitivity analysis on the value of ϵ used for frequency-based noisy candidate filtering. A larger ϵ results in a higher threshold, accepting fewer candidate labels, while a smaller ϵ leads to a lower threshold, allowing a broader range of target private label candidates. We observe that the performance remains robust across different values of the size of ϵ. Among these, we select 0.01, which shows superior performance across 4 datasets.

Scalability Analysis for Model Sizes. We conducted experiments using the CLIP-ViT-B/16 backbone. A crucial aspect of validating our method is determining whether performance scales with the backbone size. As illustrated in Table 11, increasing the backbone to CLIP-ViT-L/14@336px leads to a significant performance enhancement.

Learning Statistics of Self-Training. We present self-training learning statistics for Office31 DSLR and Office-Home Clipart under the OPDA setting in Fig. 9. A notable performance improvement occurs after a certain number of iterations.

Trade-off for training using the source samples.. We observe that incorporating the source loss term L_{src} introduces a trade-off. Table 12 demonstrates that integrating source training significantly boosts performance in partial domain adaptation (PDA) and closed-set domain adaptation (CDA) compared to self-training. However, this approach leads to higher computational demands and slightly reduced performance in open-set domain adaptation (OPDA) and open domain adaptation (ODA). Therefore, the method can be selectively employed based on the objective (Table 12).

Table 9: Ablation study with different components of our self-training approach. Delay refers to how long the teacher model's updates are delayed.

Delay	Selection Strategy		Office31				Office-Home				VisDA				DomainNet			
–	Top-k%	Balanced Top-k	OPDA	ODA	PDA	CDA	OPDA	ODA	PDA	CDA	OPDA	ODA	PDA	CDA	OPDA	ODA	PDA	CDA
Universal Classifier zero-shot			89.9	92.6	96.1	80.5	91.3	89.2	82.0	79.0	86.3	83.9	81.8	72.6	**75.4**	**76.9**	70.1	**68.9**
			91.5	94.7	97.2	82.3	93.3	90.9	84.6	81.5	87.1	85.8	85.0	75.7	73.9	74.4	72.1	67.0
✓			91.6	95.1	**97.7**	82.5	**93.7**	91.3	85.2	81.2	87.2	86.0	**85.4**	**76.1**	73.9	74.4	72.2	66.6
✓	✓		91.5	94.7	97.2	82.3	93.3	90.9	84.6	81.5	87.1	85.8	85.0	75.7	73.9	74.4	72.1	67.0
✓		✓	**91.9**	**95.2**	96.9	**82.9**	93.5	**91.4**	**85.3**	**81.8**	**87.6**	**86.0**	83.0	75.6	74.3	74.9	**74.4**	67.9

Table 10: Comparison of H-score on DomainNet to analyze the sensitivity of hyperparameter k in semantic label alignment and ϵ in frequency-based noisy candidate filtering.

k	OPDA	ODA	PDA	CDA	Avg
4	**75.9**	**77.3**	69.5	68.4	72.7
5	75.4	76.9	70.1	68.9	**72.8**
6	74.6	76.3	70.4	69.3	72.6
7	72.1	74.8	**70.8**	**69.6**	71.8
ϵ	OPDA	ODA	PDA	CDA	Avg
0.01	**75.4**	**76.9**	70.1	68.9	**72.8**
0.02	73.4	75.7	70.6	69.6	72.3
0.03	72.1	74.4	**71.0**	69.7	71.8
0.04	71.1	73.2	**71.0**	**69.8**	71.3

Table 11: Comparison of H-score with larger backbones: OH denotes Office-Home, VD denotes VisDA, and DN denotes DomainNet.

Backbone	Split Setting			
	Office31	OH	VD	DN
(a) TLSA				
ViT-B/16	85.7	85.6	82.5	75.2
ViT-L/14@336px	**92.9**	**90.3**	**84.6**	**78.9**
(b) TLSA+ST				
ViT-B/16	86.8	86.9	**84.9**	77.0
ViT-L/14@336px	**94.0**	**92.0**	83.5	**79.9**

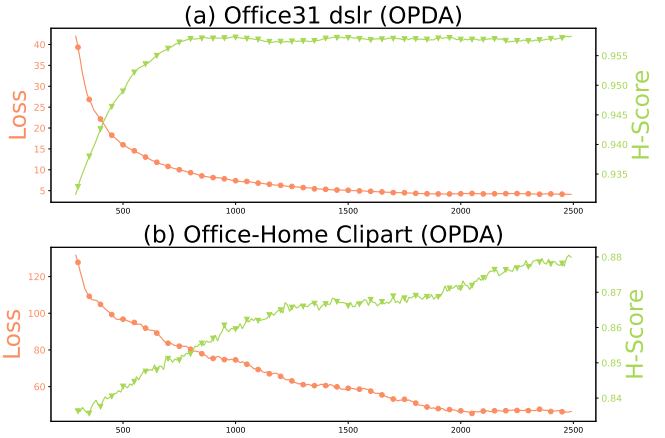

Figure 9: Learning statistics of our self-training. The x-axis value represents the iteration.

Table 12: Comparison of H-scores between self-training combined with source training and ours (self-training only).

Method	OPDA	ODA	PDA	CDA
w/ L_{src}	85.2	86.7	**85.3**	**80.0**
Ours (w/o L_{src})	**86.8**	**86.9**	84.9	77.0

6. Limitations

This study has two key limitations. First, it may not be suitable for fine-grained datasets. Because it depends on the zero-shot capabilities of CLIP and BLIP, classes that are fine-grained and underrepresented during pretraining are prone to inadequate recognition, as highlighted by Zhao et al. (2024). Furthermore, the approach does not individually address source-private class detection, which may lead to less than optimal performance within the universal set. We anticipate that our research will advance future investigations in this domain.

7. Conclusion

In this paper, we introduce a TLSA, a framework leveraging CLIP to address the UniDA problem through label space alignment. This framework utilizes a generative vision-language model to discover labels for all target domain samples and then filter out those containing source-related information. To achieve this, on a mini-batch basis, we remove trivial synonyms of source labels by synonym label alignment and remove semantically ambiguous similar labels by semantic label alignment. Subsequently, on a dataset-wide scale, frequency-based noisy candidate filtering identifies and removes unreliable labels based on occurrence patterns. The method is highly efficient both temporally and memory-wise, as it completes the entire process in a single epoch without the need for further tuning. After completing all alignment processes, we extend the existing source classes with the newly predicted target private labels to create a new *universal classifier*. This classifier demonstrates significantly better performance compared to existing methods. Additionally, by self-training with balanced top-k confident sample selection, we surpass the state-of-the-art UniDA baselines.

Appendix

8. Pseudo code

In this section, we provide a pseudo-code of our semantic label alignment approach in Alg. 1.

9. Examples of label space alignment

Fig. 10 illustrates the detailed process of two naive filtering methods, margin-based alignment and top-1 prediction-based alignment. In margin-based alignment, deriving the margin threshold τ is a non-trivial task because the class similarity between the source class and the target private class is not consistent across datasets (e.g., the case of "clipboard" in source labels and "notebook" in target private labels). In this scenario, "notebook" is consistently hindered by "clipboard" due to the lack of a significantly high margin of similarity. Therefore, τ must be adaptively adjusted. Fig. 10a demonstrates this misalignment case.

Additionally, in top-1 prediction-based alignment, in the case of "backpack" in source labels and "bag" in target private labels, since "backpack" and "bag" are not synonyms according to the WordNet hierarchy, "bag" is often chosen as the target private candidate label on a per-instance basis. Fig. 10b demonstrates this misalignment case.

Algorithm 1 Semantic Label Alignment

Require: Target samples $\mathbf{x}^t$, filtered discovered labels $\tilde{R}$, source labels C_s
Ensure: Frequency bank F

Compute target embeddings: $\mathbf{z}_v \leftarrow f_v(\mathbf{x}^t)$
Compute label embeddings: $\mathbf{z}_t \leftarrow f_t([C_s, \tilde{R}])$
Compute similarity matrix: $S \leftarrow sim(\mathbf{z}_v, \mathbf{z}_t)$
Extract top-k scores and indices: $(S_k, I_k) \leftarrow \text{topk}(S)$
Find largest gap index: $\mathbf{J} \leftarrow \arg\max_j(s_{j+1} - s_j)$
Define thresholds:
    $\tau_{\text{gap}} \leftarrow s_{\mathbf{J}}$
    $\tau_{\text{avg}} \leftarrow \mathbb{E}[S_k]$
    $\tau_{\text{set}} \leftarrow \min\{\tau_{\text{gap}}, \tau_{\text{avg}}\}$
for $i = 1$ to N **do**
    Prediction set: $C^i \leftarrow \{\mathbf{t}_{i,j} \mid j \in I_k^i,\ s_{i,j} > \tau_{\text{set}}^i\}$
    if $C^i \cap C_s = \emptyset$ **then**
        $F[r_i] \leftarrow F[r_i] + 1$
    else
        $F[p_i] \leftarrow F[p_i] + 1$
    end if
end for

10. Details of semantic label alignment

Fig. 11 presents random examples from the Office31 dataset under the DSLR OPDA setting. It shows the exact discovered labels r_i for each image i, the corresponding prediction set C^i, and the specific elements stored in the frequency bank for each case. In the prediction set, the numbers indicate the ranking based on image-text similarity.

11. Analysis of labels to be added to the frequency bank

In Section 3.4, we noted that storing BLIP's discovered label to the frequency bank is more beneficial for performance compared to storing CLIP's top-1 prediction to the frequency bank. As shown in Table 13, storing CLIP's top-1 predictions often leads to an overestimation of incorrect target private labels (e.g., overly specific or entirely incorrect classes), which in turn causes the correct target private labels (*e.g.*, 'train', 'truck', 'skateboard') to be underestimated. This imbalance ultimately results in degraded model performance. In Table 13, correct target private label is underestimated when using CLIP's top-1 prediction compared to using BLIP's discovered label.

Table 13: Comparison of predicted target private labels between label selection strategies in label space alignment in VisDA open-partial setting. When BLIP's discovered label is incorporated into the target private candidate labels, the H-score (%) is estimated at **86.3**. In contrast, using CLIP's top-1 prediction for target private candidate labels results in an H-score (%) of **80.1**.

Ours (BLIP's prediction)		**CLIP's Top-1 Prediction**	
Label	Frequency	Label	Frequency
Correct Target-Private Label			
train	3328	train	3099
truck	2215	truck	1567
skateboard	2035	skateboard	1857
Incorrect Target-Private Label			
fire truck	221	fire truck	293
van	533	van	574
dog	152	dog	96
dump truck	97	dump truck	205
skateboarder	108	skateboarder	350
food truck	136	food truck	214
pizza	113	pizza	93
umbrella	121	umbrella	87
taxi	172	taxi	388
parking meter	136	parking meter	252
jeep	113	jeep	105
fire hydrant	81	fork	94
		carriage	96
		locomotive	98
		suv	110
		police	83
		freightliner	83
		caboose	107
		trolley	83

12. Details of prompts to generative VLM

This section provides details of the question prompts used for label discovery. To ensure diversity while maintaining the same meaning, we employed five different styles of prompts. Table 14 demonstrates the detailed examples of question prompts for generative VLM.

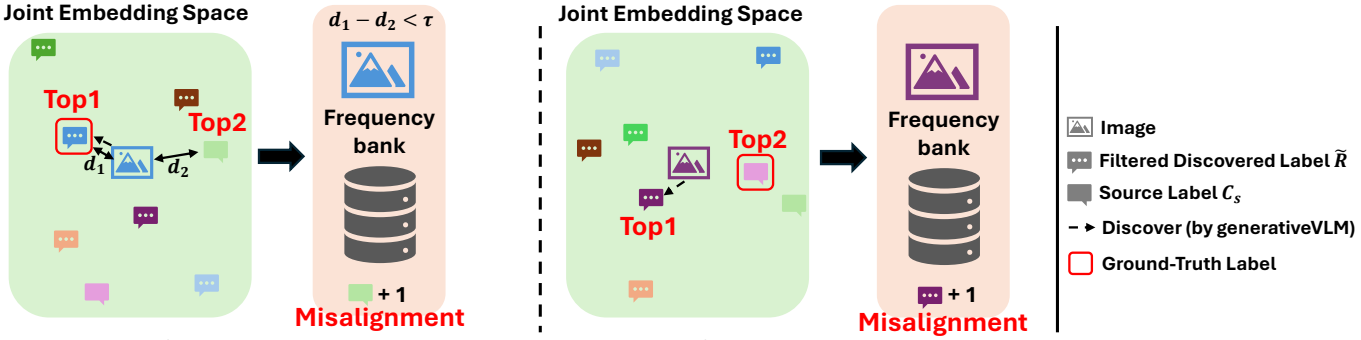

(a) An example of misalignment in margin-based alignment (b) An example of misalignment in top-1 based alignment

Figure 10: Illustrations of two naive filtering methods: (a) shows the misalignment in margin-based alignment. The example demonstrates a case where τ is not suitable for this particular dataset. (b) illustrates the misalignment in top-1 prediction-based alignment. This example shows how misalignment occurs when the source label is slightly less similar to the discovered label

Figure 11: Label space alignment with examples. This figure demonstrates the alignment process by showcasing the discovered labels, corresponding candidate prediction sets, and the final filtered results for each item. The output is stored in the frequency bank, with counts incremented by one. Discovered labels are colored in violet, and source labels are colored in orange.

(a) An Example of Source Class Samples

GT	backpack	projector	monitor
Image			
Discovered label	bag	camera	tv
Prediction set C'	1. backpack 2. bag	1. projector 2. camera	1. desktop 2. monitor
Output	backpack	projector	monitor

(b) An Example of Target-Private Class Samples

GT	printer	stapler	trash can
Image			
Discovered label	printer	stapler	recycling
Prediction set C'	1. fax machine 2. modem	1. stapler	1. recycling 2. trash can 3. recycle bin
Output	printer	stapler	recycling

Table 14: Examples of prompts used for generative VLM.

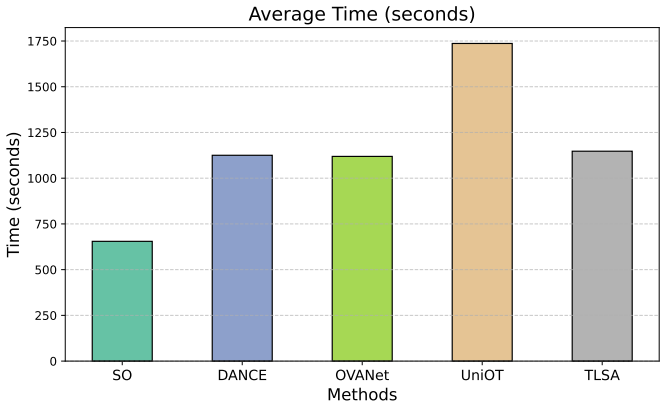

Figure 12: Average time spent on adaptation.

"What is the exact name of the object in the painting? Please tell me."
"What can you identify in the illustration? Please tell me in a word."
"What is the specific name of the object captured in the photograph? Please tell me."
"What appears in the picture with its accurate name in the drawing? Please tell me."
"What is portrayed in the photo with its exact name? Please tell me."

13. Time complexity of our method

This section explains the time complexity of our method. In Fig. 12, despite utilizing two VLMs, our approach adopts a training-free framework, resulting in minimal overhead compared to existing works. Moreover, it demonstrates faster adaptation than clustering-based methods (Chang et al., 2022).

14. Details of main results

This section details the experimental results (H-score, H^3-score) for domain-to-domain. Table 16 through Table 26 offer a comprehensive comparison between baseline methods and the proposed approach using the CLIP ViT-B/16 backbone.

Table 15: Office31 ViT-B/16 OPDA

Methods	A2D	A2W	D2A	D2W	W2A	W2D	Avg
H-score							
SO	84.4	79.0	88.1	93.3	80.2	89.8	85.8
DANCE	91.6	84.7	**93.7**	**95.8**	87.8	**96.4**	91.7
OVANet	86.8	76.1	90.1	94.9	91.0	95.2	89.0
UniOT	78.5	73.4	82.5	88.4	83.0	88.1	82.3
CLIP-Distill	81.6	81.1	87.7	81.0	87.7	81.8	83.5
MemSPM+DCC	88.0	84.6	88.7	87.6	87.9	94.3	88.5
TLSA	92.7	86.8	89.7	86.8	89.7	92.7	89.9
TLSA+ST	**95.4**	**88.7**	91.5	88.7	**91.5**	95.4	**91.9**
H^3-score							
SO	85.6	81.7	78.5	91.4	74.1	89.2	83.4
DANCE	90.4	85.7	81.4	**93.0**	78.3	**93.4**	**87.0**
OVANet	87.2	79.6	79.5	92.4	80.0	92.6	85.2
UniOT	80.5	76.9	75.2	88.5	75.4	87.7	80.7
CLIP-Distill	83.7	83.2	78.2	83.2	78.2	83.8	81.7
TLSA	**91.1**	**87.1**	79.4	87.1	79.4	91.1	85.9
TLSA+ST	88.7	85.2	**81.9**	85.2	**81.9**	88.7	85.3

Table 16: Office31 ViT-B/16 ODA

Methods	A2D	A2W	D2A	D2W	W2A	W2D	Avg
H-score							
SO	87.2	87.9	85.1	90.7	84.1	86.0	86.8
DANCE	92.4	89.3	93.4	96.7	91.7	**95.6**	93.2
OVANet	86.7	80.4	91.7	**97.4**	84.4	95.1	89.3
UniOT	91.4	91.0	92.4	96.8	94.2	97.7	93.9
CLIP-Distill	80.1	79.7	88.0	81.2	90.2	86.5	84.3
TLSA	92.2	91.7	94.1	91.7	94.1	92.2	92.7
TLSA+Self training	**94.3**	**95.4**	**95.9**	95.4	**95.9**	94.3	**95.2**
H^3-score							
SO	87.8	88.8	80.5	90.6	79.9	87.0	85.8
DANCE	91.3	89.7	85.3	94.6	84.3	**93.4**	89.8
OVANet	87.5	83.5	84.4	**95.0**	80.1	93.1	87.3
UniOT	90.7	89.7	83.8	94.2	85.1	95.5	89.8
CLIP-Distill	82.9	83.0	82.2	84.1	83.4	87.4	83.8
TLSA	**91.2**	91.1	85.7	91.1	85.7	91.2	89.3
TLSA+ST	90.9	**91.6**	**87.1**	91.6	**87.1**	90.9	**89.9**

Table 17: Office31 ViT-B/16 PDA

Methods	A2D	A2W	D2A	D2W	W2A	W2D	Avg
H-score							
SO	77.0	67.6	87.2	96.9	78.5	95.4	83.7
DANCE	51.7	49.3	86.2	89.3	67.2	**99.0**	73.8
OVANet	74.6	64.4	87.7	97.2	82.7	97.6	84.0
UniOT	28.9	26.4	27.8	38.1	29.5	38.3	31.5
CLIP-Distill	82.6	82.7	91.5	82.3	92.1	82.6	85.6
TLSA	92.7	86.8	89.7	86.8	89.7	92.7	89.9
TLSA+ST	**96.2**	**98.4**	**96.1**	**98.4**	**96.1**	96.2	**96.9**

Table 18: Office31 ViT-B/16 CDA

Methods	A2D	A2W	D2A	D2W	W2A	W2D	Avg
H-score							
SO	63.4	57.5	58.1	93.3	56.1	96.2	70.8
DANCE	58.5	50.7	53.7	93.3	52.3	97.6	67.7
OVANet	56.5	51.8	51.3	89.1	51.2	95.7	65.9
UniOT	51.9	49.8	48.4	65.3	46.2	63.7	54.2
CLIP-Distill	75.5	72.0	73.6	71.4	74.5	75.4	73.7
TLSA	82.7	80.5	79.4	80.5	79.4	82.7	79.0
TLSA+ST	**84.6**	**84.0**	**80.1**	**84.0**	**80.1**	**84.6**	**82.9**

Table 19: Office-Home ViT-B/16 OPDA

Methods	A2C	A2P	A2R	C2A	C2P	C2R	P2A	P2C	P2R	R2A	R2C	R2P	Avg
H-score													
SO	69.8	80.3	83.8	80.5	81.5	85.3	77.5	71.2	84.7	80.6	76.0	77.6	79.0
DANCE	78.0	86.4	87.1	81.1	85.2	85.6	82.4	79.9	90.5	83.6	79.6	84.1	83.6
OVANet	72.7	88.0	86.4	80.6	84.0	85.3	75.2	63.6	89.1	81.8	74.4	85.0	80.5
UniOT	85.5	89.8	91.1	79.9	87.3	89.3	80.8	83.5	88.9	83.5	84.3	91.6	86.3
CLIP-Distill	81.4	79.6	86.1	87.9	80.3	86.7	87.0	81.3	91.0	87.0	81.9	86.8	84.7
MemSPM+DCC	78.1	90.3	90.7	81.9	90.5	88.3	79.2	77.4	87.8	78.8	76.2	91.6	84.2
TLSA	87.4	95.2	95.8	86.8	95.2	95.8	86.8	87.4	95.8	86.8	87.4	95.2	91.3
TLSA+ST	**90.2**	**96.3**	**96.7**	**90.6**	**96.3**	**96.7**	**90.6**	**90.2**	**96.7**	**90.6**	**90.2**	**96.3**	**93.4**
H^3-score													
SO	67.5	82.4	82.7	73.7	83.2	83.7	71.9	68.4	83.3	73.7	71.3	80.5	76.9
DANCE	72.4	86.6	84.8	74.0	85.8	83.8	74.7	73.5	86.9	75.4	73.3	85.0	79.7
OVANet	69.3	87.7	84.4	73.7	85.0	83.7	70.6	63.5	86.1	74.4	70.3	85.7	77.9
UniOT	78.9	89.4	88.1	75.9	87.9	87.1	76.2	76.9	86.6	77.8	77.9	90.5	82.8
CLIP-Distill	74.4	81.9	84.2	77.6	82.4	84.6	77.1	74.3	87.3	77.1	74.6	86.9	80.2
TLSA	79.8	92.2	89.5	76.8	92.7	89.5	76.8	79.8	89.5	76.8	79.8	92.2	84.6
TLSA+ST	**85.5**	**93.9**	**94.1**	**87.5**	**93.9**	**94.1**	**87.5**	**85.5**	**94.1**	**87.5**	**85.5**	**93.9**	**90.2**

Table 20: Office-Home ViT-B/16 ODA

Methods	A2C	A2P	A2R	C2A	C2P	C2R	P2A	P2C	P2R	R2A	R2C	R2P	Avg
H-score													
SO	69.6	77.3	80.5	76.8	81.0	82.2	70.2	69.7	81.4	78.7	73.2	77.1	76.5
DANCE	75.2	81.5	82.9	76.2	77.1	81.6	70.2	71.5	85.6	80.0	74.8	82.6	78.3
OVANet	71.6	81.7	82.7	76.5	83.3	81.6	64.0	56.9	84.1	78.6	70.5	84.4	76.3
UniOT	81.0	85.9	85.0	76.8	85.5	83.9	72.1	77.8	83.7	80.4	79.3	89.7	81.7
CLIP-Distill	77.3	79.1	84.6	83.4	79.7	85.1	79.6	75.9	88.6	79.7	76.9	85.9	81.3
MemSPM+DCC	69.7	83.2	85.2	72.0	79.2	81.2	72.3	66.7	85.2	72.7	66.0	84.5	76.5
TLSA	85.5	92.3	93.9	85.1	92.3	93.9	85.1	85.5	93.9	85.1	85.5	92.3	89.2
TLSA+ST	**89.2**	**94.4**	**94.2**	**88.0**	**94.4**	**94.2**	**88.0**	**89.2**	**94.2**	**88.0**	**89.2**	**94.4**	**91.4**
H^3-score													
SO	67.4	80.3	80.5	71.5	82.9	81.7	67.6	67.5	81.2	72.6	69.6	80.2	75.2
DANCE	70.8	83.3	82.1	71.2	80.1	81.3	67.6	68.6	83.9	73.4	70.5	84.1	76.4
OVANet	68.7	83.4	82.0	71.4	84.5	81.3	63.7	58.9	82.9	72.6	68.0	85.2	75.2
UniOT	75.7	86.6	83.9	73.4	86.8	83.3	70.2	73.7	83.1	76.0	74.6	89.1	79.7
CLIP-Distill	72.0	81.6	83.3	75.2	82.0	83.6	73.1	71.2	85.8	73.2	71.8	86.3	78.3
TLSA	78.7	90.4	88.3	75.9	90.4	88.3	75.9	78.7	88.3	75.9	78.7	90.4	83.3
TLSA+ST	**85.0**	**92.8**	**92.3**	**85.7**	**92.8**	**92.3**	**85.7**	**85.0**	**92.3**	**85.7**	**85.0**	**92.8**	**89.0**

Table 21: Office-Home ViT-B/16 PDA

Methods	A2C	A2P	A2R	C2A	C2P	C2R	P2A	P2C	P2R	R2A	R2C	R2P	Avg
H-score													
SO	37.8	58.5	63.7	38.6	56.4	59.4	41.0	32.9	68.5	50.2	43.4	71.1	51.8
DANCE	34.3	52.6	66.0	30.2	41.5	59.1	30.7	19.9	68.2	47.9	39.5	72.4	46.8
OVANet	51.5	62.7	73.1	52.3	59.4	65.7	44.8	35.4	73.3	61.7	49.1	76.8	58.8
UniOT	31.8	34.3	31.1	26.0	32.2	29.4	26.9	30.0	33.1	36.9	31.5	38.4	31.8
CLIP-Distill	64.9	86.7	87.6	71.5	85.6	86.5	63.3	57.2	82.9	65.7	59.0	82.5	74.4
MemSPM+DCC	64.7	81.1	84.5	74.8	74.7	77.5	58.7	60.3	84.2	70.3	77.2	85.8	74.5
TLSA	74.5	**87.8**	90.4	75.3	**87.8**	90.4	75.3	74.5	90.4	75.3	74.5	**87.8**	**82.0**
TLSA+ST	**79.2**	86.3	**93.5**	**82.2**	86.3	**93.5**	**82.2**	**79.2**	**93.5**	**82.2**	**79.2**	86.3	**85.3**

Table 22: Office-Home ViT-B/16 CDA

Methods	A2C	A2P	A2R	C2A	C2P	C2R	P2A	P2C	P2R	R2A	R2C	R2P	Avg
H-score													
SO	31.3	57.0	59.8	36.8	60.9	56.5	35.6	28.3	64.9	50.2	36.3	77.5	49.6
DANCE	31.1	57.1	60.6	36.7	58.3	56.7	33.1	28.5	64.6	50.5	36.2	78.8	49.4
OVANet	41.5	60.5	70.1	49.8	61.6	64.2	42.3	30.7	70.4	60.2	40.8	81.5	56.1
UniOT	41.4	46.9	50.9	41.7	50.1	50.6	36.8	38.0	50.0	46.2	42.9	61.5	46.4
CLIP-Distill	53.1	85.9	83.2	65.1	84.9	82.6	59.2	45.7	78.5	60.4	47.8	82.2	69.0
TLSA	66.4	87.2	88.2	74.2	87.2	88.2	74.2	66.4	88.2	74.2	66.4	87.2	79.0
TLSA+ST	**71.3**	**88.6**	**89.9**	**77.3**	**88.6**	**89.9**	**77.3**	**71.3**	**89.9**	**77.3**	**71.3**	**88.6**	**81.8**

Table 23: DomainNet ViT-B/16 OPDA

Methods	P2R	P2S	R2P	R2S	S2P	S2R	Avg
H-score							
SO	64.2	50.2	53.1	52.1	48.3	67.1	55.8
DANCE	64.2	50.1	50.8	51.2	47.4	67.2	55.1
OVANet	68.2	58.6	60.5	59.1	56.9	68.6	62.0
UniOT	71.4	62.8	62.5	64.6	59.5	72.7	65.6
CLIP-Distill	74.1	61.6	58.5	60.2	59.7	74.8	64.8
MemSPM+DCC	62.4	52.8	58.5	53.3	50.4	62.6	56.7
TLSA	**83.6**	**71.2**	**71.3**	**71.2**	**71.3**	**83.6**	**75.4**
TLSA+ST	82.3	69.4	71.2	69.4	71.2	82.3	74.3
H^3-score							
SO	69.3	52.5	57.2	53.8	53.4	71.5	59.6
DANCE	69.3	52.4	55.4	53.2	52.6	71.5	59.1
OVANet	72.3	58.3	62.7	58.6	60.1	72.6	64.1
UniOT	73.9	61.6	64.0	63.3	61.6	75.1	66.6
CLIP-Distill	76.6	60.2	61.2	59.4	62.1	77.1	66.1
TLSA	83.1	**69.8**	66.1	**69.8**	66.1	83.1	73.1
TLSA+ST	**84.0**	69.2	**72.9**	69.2	**72.9**	**84.0**	**75.4**

Table 24: DomainNet ViT-B/16 ODA

Methods	P2R	P2S	R2P	R2S	S2P	S2R	Avg
H-score							
SO	68.5	55.0	57.0	56.6	51.3	70.0	59.7
DANCE	68.6	54.7	55.5	56.3	51.1	70.2	59.4
OVANet	70.4	61.4	62.5	62.1	59.4	70.6	64.4
UniOT	76.1	66.9	66.8	68.2	63.3	75.3	69.4
CLIP-Distill	76.2	63.6	59.7	62.4	61.6	76.5	66.7
TLSA	**85.6**	**72.9**	**72.1**	**72.9**	**72.1**	**85.6**	**76.9**
TLSA+ST	83.1	70.4	71.2	70.4	71.2	83.1	74.9
H^3-score							
SO	72.2	56.6	59.6	57.8	55.3	73.3	62.5
DANCE	72.3	56.5	58.5	57.6	55.2	73.4	62.2
OVANet	73.7	61.0	63.4	61.5	61.3	73.8	65.8
UniOT	76.7	65.0	66.3	66.3	63.6	76.3	69.0
CLIP-Distill	77.7	62.5	61.5	61.7	62.8	77.9	67.4
TLSA	83.7	68.1	69.5	68.1	69.5	83.7	73.8
TLSA+ST	**83.9**	**70.3**	**72.3**	**70.3**	**72.3**	**83.9**	**75.5**

Table 25: DomainNet ViT-B/16 PDA

Methods	P2R	P2S	R2P	R2S	S2P	S2R	Avg
H-score							
SO	44.4	26.5	30.0	28.6	24.0	44.0	32.9
DANCE	43.2	25.3	26.3	25.4	20.2	39.8	30.0
OVANet	55.8	36.9	41.1	39.1	38.6	58.4	45.0
UniOT	46.5	39.4	39.1	41.4	33.6	45.2	40.9
CLIP-Distill	85.0	75.0	49.1	47.9	46.4	75.0	63.1
TLSA	84.6	64.7	60.9	64.7	60.9	84.6	70.1
TLSA+ST	**86.8**	**70.0**	**66.4**	**70.0**	**66.4**	**86.8**	**74.4**

Table 26: DomainNet ViT-B/16 CDA

Methods	P2R	P2S	R2P	R2S	S2P	S2R	Avg
H-score							
SO	46.9	26.6	30.4	29.3	26.7	48.8	34.8
DANCE	46.7	26.5	29.7	28.3	26.1	47.1	34.1
OVANet	57.6	36.9	40.9	39.7	41.2	60.8	46.2
UniOT	60.0	47.1	46.8	49.7	44.6	60.9	51.5
CLIP-Distill	71.3	42.9	39.5	42.3	40.2	71.5	51.3
TLSA	**83.7**	**62.6**	60.3	**62.6**	60.3	**83.7**	**68.9**
TLSA+ST	81.0	61.6	**61.1**	61.6	**61.1**	81.0	67.9

References

Achiam, J., Adler, S., Agarwal, S., Ahmad, L., Akkaya, I., Aleman, F.L., Almeida, D., Altenschmidt, J., Altman, S., Anadkat, S., et al., 2023. Gpt-4 technical report. arXiv preprint arXiv:2303.08774 .

Adila, D., Shin, C., Cai, L., Sala, F., 2023. Zero-shot robustification of zero-shot models with foundation models. arXiv preprint arXiv:2309.04344 .

Amini, M.R., Feofanov, V., Pauletto, L., Hadjadj, L., Devijver, E., Maximov, Y., 2024. Self-training: A survey. Neurocomputing , 128904.

Bendale, A., Boult, T.E., 2016. Towards open set deep networks, in: Proceedings of the IEEE conference on computer vision and pattern recognition, pp. 1563–1572.

Cao, Z., Ma, L., Long, M., Wang, J., 2018. Partial adversarial domain adaptation, in: Proceedings of the European conference on computer vision (ECCV), pp. 135–150.

Cen, J., Luan, D., Zhang, S., Pei, Y., Zhang, Y., Zhao, D., Shen, S., Chen, Q., 2023. The devil is in the wrongly-classified samples: Towards unified open-set recognition. arXiv preprint arXiv:2302.04002 .

Chang, W., Shi, Y., Tuan, H., Wang, J., 2022. Unified optimal transport framework for universal domain adaptation. Advances in Neural Information Processing Systems 35, 29512–29524.

Chen, L., Lou, Y., He, J., Bai, T., Deng, M., 2022a. Geometric anchor correspondence mining with uncertainty modeling for universal domain adaptation, in: Proceedings of the IEEE/CVF Conference on Computer Vision and Pattern Recognition, pp. 16134–16143.

Chen, S., Ge, C., Tong, Z., Wang, J., Song, Y., Wang, J., Luo, P., 2022b. Adaptformer: Adapting vision transformers for scalable visual recognition. Advances in Neural Information Processing Systems 35, 16664–16678.

Deng, B., Jia, K., 2023. Universal domain adaptation from foundation models. arXiv preprint arXiv:2305.11092 .

Devlin, J., Chang, M.W., Lee, K., Toutanova, K., 2018. Bert: Pre-training of deep bidirectional transformers for language understanding. arXiv preprint arXiv:1810.04805 .

Dosovitskiy, A., Beyer, L., Kolesnikov, A., Weissenborn, D., Zhai, X., Unterthiner, T., Dehghani, M., Minderer, M., Heigold, G., Gelly, S., et al., 2020. An image is worth 16x16 words: Transformers for image recognition at scale. arXiv preprint arXiv:2010.11929 .

Esmaeilpour, S., Liu, B., Robertson, E., Shu, L., 2022. Zero-shot out-of-distribution detection based on the pre-trained model clip, in: Proceedings of the AAAI conference on artificial intelligence, pp. 6568–6576.

Fu, B., Cao, Z., Long, M., Wang, J., 2020. Learning to detect open classes for universal domain adaptation, in: Computer Vision–ECCV 2020: 16th European Conference, Glasgow, UK, August 23–28, 2020, Proceedings, Part XV 16, Springer. pp. 567–583.

Ganin, Y., Ustinova, E., Ajakan, H., Germain, P., Larochelle, H., Laviolette, F., March, M., Lempitsky, V., 2016. Domain-adversarial training of neural networks. Journal of machine learning research 17, 1–35.

Ge, Y., Ren, J., Gallagher, A., Wang, Y., Yang, M.H., Adam, H., Itti, L., Lakshminarayanan, B., Zhao, J., 2023. Improving zero-shot generalization and robustness of multi-modal models, in: Proceedings of the IEEE/CVF Conference on Computer Vision and Pattern Recognition, pp. 11093–11101.

Ge, Z., Demyanov, S., Chen, Z., Garnavi, R., 2017. Generative openmax for multi-class open set classification. arXiv preprint arXiv:1707.07418 .

Goyal, Y., Khot, T., Summers-Stay, D., Batra, D., Parikh, D., 2017. Making the v in vqa matter: Elevating the role of image understanding in visual question answering, in: Proceedings of the IEEE conference on computer vision and pattern recognition, pp. 6904–6913.

Hartigan, J.A., Wong, M.A., 1979. Algorithm as 136: A k-means clustering algorithm. Journal of the royal statistical society. series c (applied statistics) 28, 100–108.

He, K., Zhang, X., Ren, S., Sun, J., 2016. Deep residual learning for image recognition, in: Proceedings of the IEEE conference on computer vision and pattern recognition, pp. 770–778.

Jia, C., Yang, Y., Xia, Y., Chen, Y.T., Parekh, Z., Pham, H., Le, Q., Sung, Y.H., Li, Z., Duerig, T., 2021. Scaling up visual and vision-language representation learning with noisy text supervision, in: International conference on machine learning, PMLR. pp. 4904–4916.

Karim, N., Mithun, N.C., Rajvanshi, A., Chiu, H.p., Samarasekera, S., Rahnavard, N., 2023. C-sfda: A curriculum learning aided self-training framework for efficient source free domain adaptation, in: Proceedings of the IEEE/CVF Conference on Computer Vision and Pattern Recognition, pp. 24120–24131.

Kim, K., Yoon, K., In, Y., Moon, J., Kim, D., Park, C., 2024. Adaptive self-training framework for fine-grained scene graph generation. arXiv preprint arXiv:2401.09786 .

Kumar, A., Raghunathan, A., Jones, R., Ma, T., Liang, P., 2022. Fine-tuning can distort pretrained features and underperform out-of-distribution. arXiv preprint arXiv:2202.10054 .

Lai, Y., Liu, X., Zhou, T., Zhou, Y., 2023. Memory-assisted sub-prototype mining for universal domain adaptation. arXiv preprint arXiv:2310.05453 .

Li, G., Kang, G., Zhu, Y., Wei, Y., Yang, Y., 2021a. Domain consensus clustering for universal domain adaptation, in: Proceedings of the IEEE/CVF conference on computer vision and pattern recognition, pp. 9757–9766.

Li, J., Li, D., Savarese, S., Hoi, S., 2023. Blip-2: Bootstrapping language-image pre-training with frozen image encoders and large language models, in: International conference on machine learning, PMLR. pp. 19730–19742.

Li, J., Li, D., Xiong, C., Hoi, S., 2022. Blip: Bootstrapping language-image pre-training for unified vision-language understanding and generation, in: International conference on machine learning, PMLR. pp. 12888–12900.

Li, J., Selvaraju, R., Gotmare, A., Joty, S., Xiong, C., Hoi, S.C.H., 2021b. Align before fuse: Vision and language representation learning with momentum distillation. Advances in neural information processing systems 34, 9694–9705.

Liang, J., Hu, D., Feng, J., 2020. Do we really need to access the source data? source hypothesis transfer for unsupervised domain adaptation, in: International conference on machine learning, PMLR. pp. 6028–6039.

Liu, H., Li, C., Wu, Q., Lee, Y.J., 2024. Visual instruction tuning. Advances in neural information processing systems 36.

Long, M., Cao, Y., Wang, J., Jordan, M., 2015. Learning transferable features with deep adaptation networks, in: International conference on machine learning, PMLR. pp. 97–105.

Long, M., Cao, Z., Wang, J., Jordan, M.I., 2018. Conditional adversarial domain adaptation. Advances in neural information processing systems 31.

Long, M., Zhu, H., Wang, J., Jordan, M.I., 2016. Unsupervised domain adaptation with residual transfer networks. Advances in neural information processing systems 29.

Long, M., Zhu, H., Wang, J., Jordan, M.I., 2017. Deep transfer learning with joint adaptation networks, in: International conference on machine learning, PMLR. pp. 2208–2217.

Lu, Y., Shen, M., Ma, A.J., Xie, X., Lai, J.H., 2024. Mlnet: Mutual learning network with neighborhood invariance for universal domain adaptation, in: Proceedings of the AAAI Conference on Artificial Intelligence, pp. 3900–3908.

Miller, G.A., Beckwith, R., Fellbaum, C., Gross, D., Miller, K.J., 1990. Introduction to wordnet: An on-line lexical database. International journal of lexicography 3, 235–244.

Ming, Y., Cai, Z., Gu, J., Sun, Y., Li, W., Li, Y., 2022. Delving into out-of-distribution detection with vision-language representations. Advances in neural information processing systems 35, 35087–35102.

Oquab, M., Darcet, T., Moutakanni, T., Vo, H., Szafraniec, M., Khalidov, V., Fernandez, P., Haziza, D., Massa, F., El-Nouby, A., et al., 2023. Dinov2: Learning robust visual features without supervision. arXiv preprint arXiv:2304.07193 .

Oza, P., Patel, V.M., 2019. C2ae: Class conditioned auto-encoder for open-set recognition, in: Proceedings of the IEEE/CVF conference on computer vision and pattern recognition, pp. 2307–2316.

Panareda Busto, P., Gall, J., 2017. Open set domain adaptation, in: Proceedings of the IEEE international conference on computer vision, pp. 754–763.

Peng, X., Bai, Q., Xia, X., Huang, Z., Saenko, K., Wang, B., 2019. Moment matching for multi-source domain adaptation, in: Proceedings of the IEEE/CVF international conference on computer vision, pp. 1406–1415.

Peng, X., Usman, B., Kaushik, N., Hoffman, J., Wang, D., Saenko, K., 2017. Visda: The visual domain adaptation challenge. arXiv preprint arXiv:1710.06924 .

Qu, H., Hui, X., Cai, Y., Liu, J., 2024a. Lmc: Large model collaboration with cross-assessment for training-free open-set object recognition. Advances in Neural Information Processing Systems 36.

Qu, S., Zou, T., He, L., Röhrbein, F., Knoll, A., Chen, G., Jiang, C., 2024b. Lead: Learning decomposition for source-free universal domain adaptation, in: Proceedings of the IEEE/CVF Conference on Computer Vision and Pattern Recognition, pp. 23334–23343.

Qu, S., Zou, T., Röhrbein, F., Lu, C., Chen, G., Tao, D., Jiang, C., 2023a. Upcycling models under domain and category shift, in: Proceedings of the IEEE/CVF Conference on Computer Vision and Pattern Recognition, pp. 20019–20028.

Qu, S., Zou, T., Röhrbein, F., Lu, C., Chen, G., Tao, D., Jiang, C., 2023b. Upcycling models under domain and category shift, in: Proceedings of the IEEE/CVF conference on computer vision and pattern recognition, pp. 20019–20028.

Qu, S., Zou, T., Röhrbein, F., Lu, C., Chen, G., Tao, D., Jiang, C., 2024c. Glc++: Source-free universal domain adaptation through global-local clustering and contrastive affinity learning. arXiv preprint arXiv:2403.14410 .

Radford, A., Kim, J.W., Hallacy, C., Ramesh, A., Goh, G., Agarwal, S., Sastry, G., Askell, A., Mishkin, P., Clark, J., et al., 2021. Learning transferable visual models from natural language supervision, in: International conference on machine learning, PMLR. pp. 8748–8763.

Russakovsky, O., Deng, J., Su, H., Krause, J., Satheesh, S., Ma, S., Huang, Z., Karpathy, A., Khosla, A., Bernstein, M., et al., 2015. Imagenet large scale visual recognition challenge. International journal of computer vision 115, 211–252.

Saenko, K., Kulis, B., Fritz, M., Darrell, T., 2010. Adapting visual category models to new domains, in: Computer Vision–ECCV 2010: 11th European Conference on Computer Vision, Heraklion, Crete, Greece, September 5-11, 2010, Proceedings, Part IV 11, Springer. pp. 213–226.

Saito, K., Kim, D., Sclaroff, S., Saenko, K., 2020. Universal domain adaptation through self supervision. Advances in neural information processing systems 33, 16282–16292.

Saito, K., Kim, D., Teterwak, P., Feris, R., Saenko, K., 2023. Mind the backbone: Minimizing backbone distortion for robust object detection. arXiv preprint arXiv:2303.14744 .

Saito, K., Saenko, K., 2021. Ovanet: One-vs-all network for universal domain adaptation, in: Proceedings of the ieee/cvf international conference on computer vision, pp. 9000–9009.

Saito, K., Watanabe, K., Ushiku, Y., Harada, T., 2018. Maximum classifier discrepancy for unsupervised domain adaptation, in: Proceedings of the IEEE conference on computer vision and pattern recognition, pp. 3723–3732.

Scheirer, W.J., de Rezende Rocha, A., Sapkota, A., Boult, T.E., 2012. Toward open set recognition. IEEE transactions on pattern analysis and machine intelligence 35, 1757–1772.

Shu, M., Nie, W., Huang, D.A., Yu, Z., Goldstein, T., Anandkumar, A., Xiao, C., 2022. Test-time prompt tuning for zero-shot generalization in vision-language models. Advances in Neural Information Processing Systems 35, 14274–14289.

Tang, S., Su, W., Ye, M., Zhu, X., 2024. Source-free domain adaptation with frozen multimodal foundation model, in: Proceedings of the IEEE/CVF Conference on Computer Vision and Pattern Recognition, pp. 23711–23720.

Trivedi, P., Koutra, D., Thiagarajan, J.J., 2023. A closer look at model adaptation using feature distortion and simplicity bias. arXiv preprint arXiv:2303.13500 .

Tzeng, E., Hoffman, J., Saenko, K., Darrell, T., 2017. Adversarial discriminative domain adaptation, in: Proceedings of the IEEE conference on computer vision and pattern recognition, pp. 7167–7176.

Vaze, S., Han, K., Vedaldi, A., Zisserman, A., 2022. Open-set recognition: A good closed-set classifier is all you need, in: International Conference on Learning Representations. URL: https://openreview.net/forum?id=5hLP5JY9S2d.

Venkateswara, H., Eusebio, J., Chakraborty, S., Panchanathan, S., 2017. Deep hashing network for unsupervised domain adaptation, in: Proceedings of the IEEE conference on computer vision and pattern recognition, pp. 5018–5027.

Wang, H., Li, Y., Yao, H., Li, X., 2023. Clipn for zero-shot ood detection: Teaching clip to say no, in: Proceedings of the IEEE/CVF International Conference on Computer Vision, pp. 1802–1812.

Wang, Y., Zhang, L., Song, R., Li, H., Rosin, P.L., Zhang, W., 2024a. Exploiting inter-sample affinity for knowability-aware universal domain adaptation. International Journal of Computer Vision 132, 1800–1816.

Wang, Z., Liang, J., Sheng, L., He, R., Wang, Z., Tan, T., 2024b. A hard-to-beat baseline for training-free clip-based adaptation. arXiv preprint arXiv:2402.04087 .

Wortsman, M., Ilharco, G., Kim, J.W., Li, M., Kornblith, S., Roelofs, R., Lopes, R.G., Hajishirzi, H., Farhadi, A., Namkoong, H., et al., 2022. Robust fine-tuning of zero-shot models, in: Proceedings of the IEEE/CVF conference on computer vision and pattern recognition, pp. 7959–7971.

You, K., Long, M., Cao, Z., Wang, J., Jordan, M.I., 2019a. Universal domain adaptation, in: Proceedings of the IEEE/CVF conference on computer vision and pattern recognition, pp. 2720–2729.

You, K., Long, M., Cao, Z., Wang, J., Jordan, M.I., 2019b. Universal domain adaptation, in: Proceedings of the IEEE/CVF conference on computer vision and pattern recognition, pp. 2720–2729.

Zanella, M., Ben Ayed, I., 2024. On the test-time zero-shot generalization of vision-language models: Do we really need prompt learning?, in: Proceedings of the IEEE/CVF Conference on Computer Vision and Pattern Recognition, pp. 23783–23793.

Zara, G., Roy, S., Rota, P., Ricci, E., 2023. Autolabel: Clip-based framework for open-set video domain adaptation, in: Proceedings of the IEEE/CVF Conference on Computer Vision and Pattern Recognition, pp. 11504–11513.

Zhang, W., Shen, L., Foo, C.S., 2023. Rethinking the role of pre-trained networks in source-free domain adaptation, in: Proceedings of the IEEE/CVF International Conference on Computer Vision, pp. 18841–18851.

Zhao, Q., Dai, Y., Li, H., Hu, W., Zhang, F., Liu, J., 2024. Ltgc: Long-tail recognition via leveraging llms-driven generated content, in: Proceedings of the IEEE/CVF Conference on Computer Vision and Pattern Recognition, pp. 19510–19520.

Zhou, K., Yang, J., Loy, C.C., Liu, Z., 2022. Learning to prompt for vision-language models. International Journal of Computer Vision 130, 2337–2348.